Order Number 1352330

Processing of copper aluminosilicate glasses to produce glass-copper structures

Beatty, Kirk Matthew, M.S.

The University of Arizona, 1993

U·M·I
300 N. Zeeb Rd.
Ann Arbor, MI 48106

PROCESSING OF COPPER ALUMINOSILICATE GLASSES TO PRODUCE GLASS-COPPER STRUCTURES

by

Kirk Matthew Beatty

A Thesis Submitted to the Faculty of the

DEPARTMENT OF MATERIALS SCIENCE AND ENGINEERING

In Partial Fulfillment of the Requirements
For the Degree of

MASTER OF SCIENCE

In the Graduate College

THE UNIVERSITY OF ARIZONA

1 9 9 3

STATEMENT BY AUTHOR

This thesis has been submitted in partial fulfillment of requirements for an advanced degree at The University of Arizona and is deposited in the University Library to be made available to borrowers under rules of the Library.

Brief quotations from this thesis are allowable without special permission, provided that accurate acknowledgment of source is made. Requests for permission for extended quotation from or reproduction of this manuscript in whole or in part may be granted by the head of the major department or the Dean of the Graduate College when in his or her judgment the proposed use of the material is in the interests of scholarship. In all other instances, however, permission must be obtained from the author.

SIGNED: Kirk Matthew Beatty

APPROVAL BY THESIS DIRECTOR

This thesis has been approved on the date shown below:

David C. Lynch

12/7/92

David C. Lynch
Professor of Materials Science and Engineering

Date

ACKNOWLEDGEMENTS

I would like to thank Professor Lynch for his help in this thesis. He has provided motivation and useful suggestions.

Several people provided help with this thesis. Kris Law provided help with the work on the JEOL SEM. Zoe Osborne made some useful suggestions about use of the pull test method. Howard Poisl melted several batches of glass used in this thesis. Doug Taylor made the surface profile measurements using the DEKTAK IIA. Gary Smith was instrumental in my last batch of glass polishing. I am also grateful to Bueler and the assistance of those who have worked there in the polishing and mounting of glass samples. Kathy Sole proofread an early draft and provided valuable input. I would also like to thank the people in the Lynch group. I would also like to thank the University of Arizona Copper Research Center for funding this research.

Finally, I am grateful for the help and encouragement of friends and family.

TABLE OF CONTENTS

LIST OF ILLUSTRATIONS

LIST OF ILLUSTRATIONS - *Continued*

LIST OF ILLUSTRATIONS - *Continued*

LIST OF TABLES

LIST OF TABLES - *Continued*

LIST OF TABLES - *Continued*

LIST OF TABLES - *Continued*

LIST OF TABLES - *Continued*

LIST OF TABLES - *Continued*

ABSTRACT

Copper aluminosilicate (composition $Cu_2O \cdot Al_2O_3 \cdot 6SiO_2$) glass was melted in an alumina crucible at 1500°C and air cooled *in situ*. A layer of cupric oxide was grown on the polished glass surface and its thickness measured using a scanning electron microscope (SEM). The thickness of the oxide layer was found to increase parabolically with time, with a temperature dependency that was compatible with the diffusion of copper through the layer. The cupric oxide layer was reduced to copper on roughened and polished glass surfaces using a gas mixture of 3% H_2 and 97% N_2, resulting in a glass substrate coated by copper. Adherence of the copper layer to the polished glass substrate was found to be poor. However, adherence was found to increase by roughening the surface before oxidation. Additions of NiO and CaO to the base glass were not detrimental to the production of the copper film.

CHAPTER 1

INTRODUCTION

This thesis focuses on the processing of copper aluminosilicate glass to produce a glass substrate with a copper film at its surface. Historically, however, the main interest in copper aluminosilicate glass was due to its low expansion coefficient and low (relative to silica) melting point.[1] This introduction contains a brief history of investigations of copper aluminosilicate glass, reserving the more detailed treatment of the thermodynamics and kinetics of processing to Chapters 2 and 3. The direction of study presented in this thesis is described in the final section of the introduction.

1.1 Historical Background

Research into copper aluminosilicate (CuAS) glass was extended by the work of Baak and Rapp. These studies are described in their patents.[1,2,3] The patents are predominantly concerned with the potential uses of the glasses due to their low expansion coefficient and low melting point. In Patent 3,779,781 Baak and Rapp suggested uses for CuAS glasses, including making glass seals, optical mirrors, and even decorative materials. To support their claims they provided information on viscosity-temperature relationships for several glasses and data on chemical durability. The glass numbered 443 (of composition $Cu_2O{\cdot}Al_2O_3{\cdot}6SiO_2$ that will be referred to as 1-1-6) had a viscosity $\log_{10}$ of 13.4 poise at 640°C, 4 poise at 1300°, and 2.5 poise at 1600°C. They also found that they could slightly increase the chemical

durability by the addition of approximately 1% fluoride compounds. They suggested that most of the copper was in the cuprous state, which could be altered by appropriate furnace conditions. In addition they showed that zinc could be used to reduce the oxidation of the glass on the surface.[1]

Matusita and Mackenzie continued work on the thermal expansion of the copper aluminosilicate glasses. They found that the melting point of the glass could be reduced by the addition of Na_2O, though this also increased the thermal expansion coefficient. They proposed that the glass separated into a copper-rich phase and a silica rich matrix upon cooling. This would help explain the low expansion coefficient of this glass. They came to the conclusion that the Cu^+/Cu^{++} ratio did not affect the thermal expansion coefficient.[4] However this was later contradicted by the work of Matusita, Sakka and Shouji[5] who found it was significant. Matusita, Sakka, and Shouji also studied the effect of other additions to the glass including B_2O_3 and GeO. However the results were not promising; for example, there was crystallization of a yellow phase when large amounts of boron were used to replace Al_2O_3.

The work of Matusita *et al.*[5] suggested that the oxidation state of the copper in the CuAS glass had an important effect upon its properties. Yoko, Kamiya, and Sakka pursued this area of study by producing CuAS glass by two different routes to change the Cu^+/Cu^{++} ratio of the glass.[6] The first approach was to make CuAS glass by ion exchange with Na_2O-Al_2O_3-SiO_2 glass, which had a lower percentage of copper in the cuprous state, but a higher thermal expansion coefficient. The second method they employed was to make CuAS glass by the normal route (melting of

powders) and then oxidize small samples of the glass to form a copper oxide layer on the surface of the glass. They then dissolved away the copper oxide layer. This process was repeated until the cuprous/cupric ion ratio in the glass had significantly changed. Again they found that as the ratio was reduced, the thermal expansion coefficient increased.

Kamiya, Yoko, and Sakka[7] continued their investigation of the oxidation of the copper aluminosilicate glass 1-1-4 in air at 500°C. They measured the rate of oxidation by forming the oxide layer, dissolving the oxide layer using HCl, and then weighing the remaining glass. The thickness of the oxide layer was found to increase in proportion to the square root of time.

1.2 New Avenues for Study

The oxidation state of copper in copper aluminosilicate glass, and properties derived thereof, have become increasingly important in the study of copper aluminosilicate glass. For example, the oxidation state of the copper has been found to be correlated with the low expansion coefficient of the glass - the initial reason for which it was studied. It has become apparent that the variable valency of the copper opens up new avenues for study. The cupric oxide layer that forms on the glass at temperatures near 500°C is a novel property. It is possible to produce metal/glass structures if the cupric oxide layer is reduced to the metallic state. A metallic copper layer attached to a glass substrate could be used in the electronics industry for electrical interconnects. It is also been suggested that the copper/glass structures

could be used as an artistic medium that could be incorporated into cookware or decorative building panels.[8] Research is necessary, however, in order to ascertain what structures are realistic and possible. Necessary work includes extending the work of Kamiya *et al.* on the oxidation of the CuAS glass, and methods of reducing the resulting cupric oxide layer. It is desirable to find alternate glass compositions that will form the cupric oxide layer, but will have different properties such as a lower melting point or differing thermal expansion coefficient. Another problem to be addressed is the mechanical and chemical stability of copper/glass structures created. A major concern in many applications is the adherence of the copper layer to the glass.[9]

This thesis is an investigation into the production of a copper/copper aluminosilicate glass structure through the route of glass oxidation followed by reduction. Chapters 2 and 3 cover background material for the thermodynamics of the formation of copper layers, the mechanisms involved and their associated kinetics, and the practical methods for improving and measuring the adhesion of a metallic layer to glass. The experimental portion of this thesis involves the creation of a mechanically and chemically stable structure comprising a film of copper on copper aluminosilicate glass by processing of the copper aluminosilicate glass.

CHAPTER 2

PRODUCTION OF Cu LAYER ON CuAS GLASS

Copper aluminosilicate glass with copper in the cuprous (Cu^+) state can be oxidized at temperatures near 500°C to produce a cupric (Cu^{++}) oxide layer on the CuAS glass.[1,6,7] Once this surface oxide layer is reduced to metal the result is a CuAS glass substrate with a surface layer of copper. The following three steps are suggested for the production of glass/copper structures:

(1) production of glass with copper in the cuprous state,

(2) oxidation of the glass to produce a cupric oxide layer,

(3) reduction of the cupric oxide layer to copper.

The creation of copper/CuAS glass structures using these three steps will only be successful if each step is thermodynamically favorable and proceeds at a reasonable rate. This chapter considers the thermodynamics of processes 1,2 and 3 and also the kinetics of process 2. The kinetics of process 3 are considered in Chapter 5 which discusses experimental results.

2.1 Equilibrium of Oxides in CuAS Glass Processing

For each of the processing steps listed above it is important to determine the stable oxidation state of copper. A simplifying assumption is that copper is always associated with oxygen, and is in the Cu^+ state when associated with Cu_2O and in the Cu^{++} state when associated with CuO. The relevant equations for copper will therefore involve oxides of copper.

Assuming the copper is in the form of cuprous and cupric oxides dissolved in the glass and the oxygen in the melt is in equilibrium with the partial pressure of oxygen over the melt, the first process can be written:[10,11]

$$2Cu_2O_{(glass)} + O_{2_{(glass)}} = 4CuO_{(glass)} \quad (2.1)$$

The equilibrium constant K for the reaction is:[12]

$$K = \frac{[a_{CuO_{(glass)}}]^4}{[P_{O_2}][a_{Cu_2O_{(glass)}}]^2} \quad (2.2)$$

The change in Gibbs energy for this reaction is:

$$\Delta G = \Delta G^o - RTlnK \quad (2.3)$$

Where ΔG° is the Gibbs energy change in the standard state. Direct application of equation (2.2) and equation (2.3) is not possible since the activities of cuprous and cupric oxides in the glass are not known. In fact, the Gibbs energy for the reaction involving CuO and Cu_2O in their standard states is not presently known above 1100°C (see Figure 2.1 which shows an Ellingham diagram for the oxides present in CuAS glass).[37] The activities of cuprous and cupric oxide in the glass can be modeled using ideal dilution. For example, one could assume for cuprous oxide (omitting subscripts for glass):

$$a_{CuO} = X_{CuO} \quad (2.4)$$

where X_{CuO} refers to molar concentration of CuO.

Defining the total molar concentration of the copper oxides as:

$$M = 2X_{CuO} + X_{Cu_2O} \tag{2.5}$$

the reaction constant K is found to be

$$\frac{[X_{CuO}]^4[M-\frac{X_{CuO}}{2}]^{-2}[1+\frac{X_{CuO}}{2}]^2}{PO_2} = K \tag{2.6}$$

There is existing data on the ratios of the copper in the cuprous (Cu^{++}) state to total copper, from which the molar concentrations can be found for both the cuprous and cupric state.[7] This thermodynamic model can be fitted to existing data to predict the amount of copper in the cuprous state as a function of temperature.

It has been assumed that the activity of oxygen in the melt was related to the partial pressure of oxygen in the melt. In practice, however, the activity of oxygen in the melt can be shifted substantially from the equilibrium value. It has been found glasses with a high basicity have a higher activity of oxygen. This is expected to shift the equilibrium of equation (2.1) to the right promoting the formation of cuprous oxide. This has been found for copper glasses. Copper glasses with higher basicity have more copper in the higher oxidation state.[10]

The second process was studied by Kamiya *et al.*[7] If written in terms of the oxides their equation becomes:

$$Cu_2O_{(glass)} + O_{2(g)} = CuO_{(glass)} + CuO_{layer} \qquad (2.7)$$

Application of thermodynamics to this reaction is problematic. Glass is not an equilibrium structure below the glass transformation temperature. Therefore the application of thermodynamics necessitates assumptions about the structure of the glass. In fact the particulars of the glass must be known, since the processing history of the glass affects the properties of the glass such as the state of internal stress, extent of oxidation, or even the extent of phase separation.[13] However, comparison of the pure oxide reaction may provide a crude guideline as to which reactions are reasonable. The final verdict must depend on experimental measurements.

The third processing step can be modeled as including the reduction of cupric oxide to cuprous oxide:

$$4CuO_{(layer)} + 2H_{2(g)} = 2Cu_2O(layer) + 2H_2O_{(g)} \qquad (2.8)$$

and the further reduction of cuprous oxide to copper:

$$2Cu_2O_{(layer)} + 2H_{2(g)} = 4Cu_{(layer)} + 2H_2O_{(g)} \qquad (2.9)$$

Kamiya's work indicated that the cupric oxide that formed on the surface of CuAS glass was in its pure form. If the oxide layer does not have significant impurities, then use can be made of an Ellingham diagram to determine at what temperatures and pressures of hydrogen this reaction should proceed.

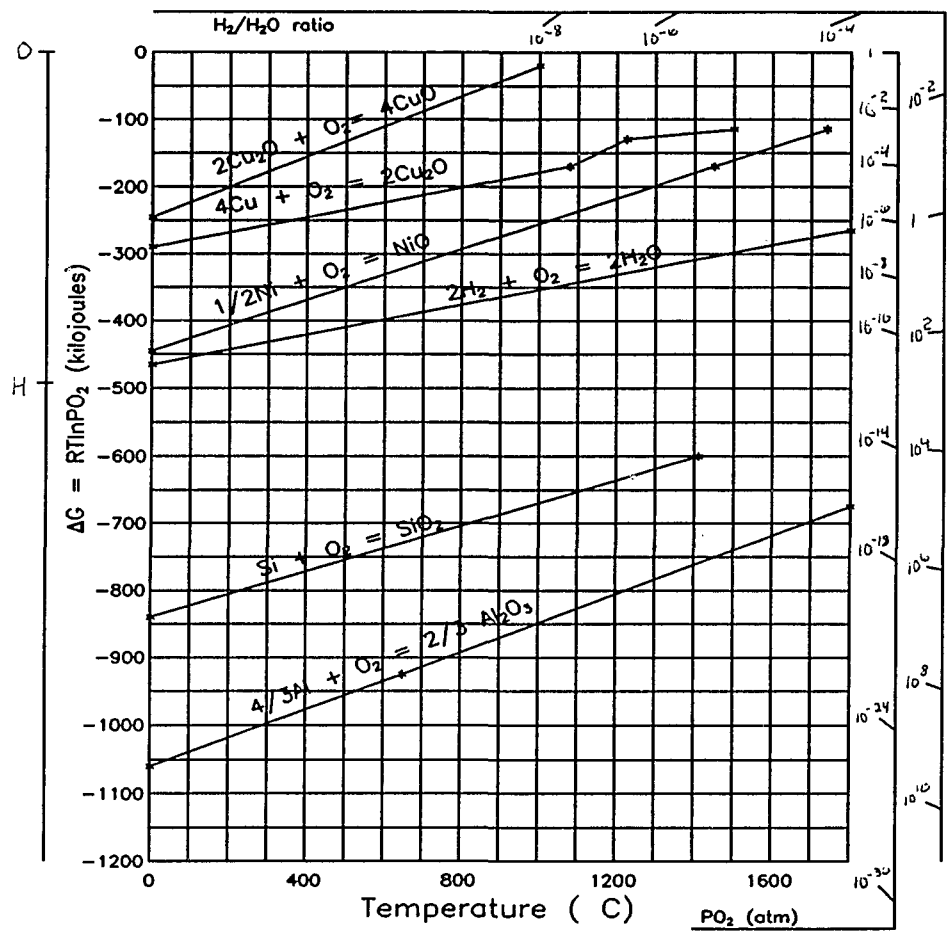

Figure 2.1 Ellingham diagram for copper, aluminum and silicon oxides.

2.2 Kinetics of Oxide Scale Formation on CuAS Glass

In this section the kinetics of the second process, the oxidation of the glass, is reviewed. The section begins with the model developed by Kamiya *et al.* to explain their experimental investigation of the process. Since the mechanisms that Kamiya *et al.* propose is similar to the mechanism involved in the oxidation of metals, the theory for the oxidation of metals is reviewed, starting with a model using uncharged defects, and progressing to Wagner's theory for the oxidation of metals.

In order to determine an expression for the growth rate of a cupric oxide layer on copper aluminosilicate glass, a description of the mechanisms involved is needed. The most extensive work on the process was done by Kamiya *et al.*[7] They found the result of the oxidation was the formation of a cupric oxide layer, and a decrease of ions in the cuprous state in the glass. Kamiya *et al.* proposed for the oxidation of CuAs glass, that oxidation was controlled by the movement of cations through the cupric oxide layer. The reactions they proposed were:

$$2Cu^{+}(glass) \rightarrow Cu^{2+}(glass) + Cu^{2+}(surface) + 2e^{-} \tag{2.10}$$

$$\frac{1}{2}O_2(surface) + 2e^{-} \rightarrow O^{2-} \tag{2.11}$$

$$Cu^{2+}(surface) + O^{2-} \rightarrow CuO(surface) \tag{2.12}$$

Adding the individual steps gives the total reaction:

$$2Cu^{+}(glass)+\frac{1}{2}O_2(surface)\rightarrow Cu^{2+}(glass)+CuO(surface) \qquad (2.13)$$

The above chemical reactions do not indicate the placement of the cations in the oxide layer. In order to indicate which sites are involved the more descriptive Kroger-Vink notation is used.[14] A short description of the notation, and definition of some of the symbols used in this section are given in Appendix A. If CuO is taken to be the standard matrix, and retaining chemical equations for reactions in the glass, and if the migrating copper vacancy is assumed to be V''_{Cu} one can write another set of equations for the reactions:

$$\frac{1}{2}O_2 = V''_{Cu\ (oxide)} + 2\dot{h} + O_{o\ (oxide)} \qquad (2.14)$$

$$V''_{Cu(oxide)}+\ddot{Cu}_{interface}\leftrightarrows Cu_{Cu(oxide)} \qquad (2.15)$$

$$\dot{Cu}_{glass}+\dot{h}\leftrightarrows\ddot{Cu}_{glass} \qquad (2.16)$$

which gives a net reaction:

$$2\dot{Cu}_{glass} + \frac{1}{2}O_2 \leftrightarrows Cu_{Cu(oxide)} + O_{O(oxide)}+\ddot{Cu}_{glass} \qquad (2.17)$$

As the oxide layer increases in thickness the concentration of defects will be related to the oxygen partial pressure using equation (2.14) to arrive at the following:

$$K = \frac{[V''_{Cu}][\dot{h}]^2}{PO_2^{1/2}} \qquad (2.18)$$

It is often possible to impose a restriction on the relationship between the vacancy and hole concentrations. This leads to the concentration of vacancies being determined only by the pressure of oxygen at the surface of the oxide.

The remaining difficulty is the treatment of the transport of copper across glass/oxide interface. Depletion of copper from the glass could affect the concentration of vacancies in the oxide layer. This would affect the diffusion through the oxide layer and therefore the growth rate. Therefore in order to describe the growth of the oxide layer, the interactions at the glass/oxide interface and the rate of diffusion in the glass must be known. However, it is known that copper diffuses very quickly through copper aluminosilicate glasses at 550°C from the work of Kamiya.[7] Therefore it is reasonable to assume that the steady state conditions are achieved at the glass oxide interface.

The model of Kamiya's which was presented bears a strong resemblance to the processes involved in the oxidation of metals. The oxidation of many metals, including copper under suitable conditions, can produce a compact pore free oxide layer. The growth of the oxide layer depends on the reaction between the metal and the metal oxide layer, migration of metal and/or oxygen ions through the oxide layer,

and reaction with the atmosphere at the surface of the oxide. Often it is found that the rate limiting step of the growth of the oxide layer is the diffusion of the ions through the oxide layer.[15,16] The driving force for the migration of the ions is the energy of formation of the oxide from the metal and oxygen gas.

Since the reactions at the surfaces of the oxide are not rate limiting an equilibrium will be established at the interface and surface of the oxide with the metal and oxygen atmosphere respectively. At the surface of the oxide layer an equilibrium will be established by a reaction between oxygen in the gas and vacancies within the oxide.

In Kröger-Vink notation the production of vacancies of charge p at the surface is given by the equation:[17]

$$\frac{1}{2}O_2(g) \leftrightarrows O_O + V_M^{p-} + p\dot{h} \qquad (2.19)$$

where p is the charge of the vacancy, $\dot{h}$ is an electron hole, and O_o is oxygen on an oxygen site (see Appendix A for a short description of the Kröger-Vink notation). At the metal-oxide interface, there will be a different equilibrium concentration of vacancies in the oxide layer which is established. Therefore there is a gradient in the concentration of defects established from the metal-oxide interface to the surface of the oxide layer. Figure 2.2 shows a schematic for metal vacancy concentration across an oxide layer. If the growth of the oxide layer depends only on cations vacancies that are not charged (p=0 in equation (2.19)) the growth of the oxide layer

can be determined from mass transport equations for the vacancies. The flow of the vacancies will have the same magnitude but opposite sign of the flow of metal cations.[18] If the diffusion coefficient of the metal vacancies does not depend on their concentration, Fick's first law of diffusion gives:

$$J_M^S = -J_V^S = D_v\left(\frac{\partial[V_M]}{\partial x}\right)_{x=w(t)} \tag{2.20}$$

where J_m is the flux of the metal cations in the oxide, D_v is the diffusion coefficient of the metal vacancies in the oxide, and the partial derivative is the change of concentration of vacancies with respect to distance. At the surface the flux of the metal must match the growth of the oxide layer therefore:

$$J_M^S = c_M^S \frac{\partial w}{\partial t} \tag{2.21}$$

where c is the concentration, the lower subscript indicating concentration of metal, the superscript designating the surface of the oxide layer. Combing equations (2.20) and (2.21) leads to:

$$D_v\left(\frac{\partial[V_M]}{\partial x}\right)_{x=w(t)} = c_M^S \frac{\partial w}{\partial t} \tag{2.22}$$

Assuming the gradient of the concentration scales with the width of the oxide layer:

$$\left(\frac{\partial[V_M]}{\partial x}\right)_{x=w(t)} = \gamma \frac{[V_M]_s - [V_M]_i}{w} \tag{2.23}$$

where γ is a constant that does not depend on the width of the layer. γ is the ratio of the concentration gradient of vacancies at the surface to the gradient of vacancies across the oxide layer assuming a linear profile. Combining equations (2.22) and (2.23) leads to:

$$wdw = D_v \gamma \frac{[V_M]_s - [V_M]_i}{c_M^S} dt \tag{2.24}$$

It has been assumed the diffusion of the metal depends only on neutral vacancies. This gives the additional relationship:

$$D_M c_M^S = D_v [V_M]_s \tag{2.25}$$

combining equations (2.24) and (2.25) leads to:

$$wdw = D_M \gamma \frac{[V_M]_s - [V_M]_i}{[V_M]_s} dt \tag{2.26}$$

Integrating equation (2.26) the width of the oxide layer at some time t is found to be:

$$w = \sqrt{2D_M\gamma\frac{[V_M]_s-[V_M]_i}{[V_M]_s}t} \qquad (2.27)$$

In Appendix B it is shown that the value of γ approaches unity if the differences in the vacancy concentrations is small in comparison to the concentration of the metal ion. Equation (2.27) applies to neutral vacancies that are not affected by an electric field.

However, in general there are several types of diffusing species, each with an associated charge. Wagner treated the case were growth of an oxide layer was controlled by the diffusion of ions through the oxide.[17] Since the species have differing mobilities and have a charge, a separation of charge will be created. Charged ions will be affected not only by the gradient of the chemical potential across the oxide, but also by the gradient of the electric potential across the oxide. This leads to:

$$j_i = \frac{-c_i v_i}{z_i e}\left(\frac{\partial \mu_i}{\partial x} + z_i e\frac{\partial \phi}{\partial x}\right) \qquad (2.28)$$

where z_i is the valence of the particle, μ_i is the chemical potential, ϕ is the electric potential, e is the electronic charge, c_i is the particle concentration, and v_i is their

mobility. A steady state condition is reached because the separation of charge creates an electric field that opposes further separation. Assuming that no net current flows through the sample, and making use of transport properties the electric field can be eliminated from this equation. From this a reaction rate is derived that depends only on the chemical potential gradient of the different species and their associated transport numbers and the reciprocal of the thickness of the oxide scale. If the migrating species do not interact, the result is:[17]

$$w^2 = 2k_p't \tag{2.29}$$

where k' is the parabolic rate constant for the growth of an oxide film, t is the time of oxidation, and w is the width of the layer. If the activity of the defects can be calculated by their respective concentrations the parabolic rate constant will depend only on the diffusion coefficient of the relevant defects. Further if the diffusion coefficient of the relevant defects do not depend on their charge the and the concentrations of vacancies at the metal are negligible, then the diffusion coefficient and parabolic rate constant are related by the simple relation:[17]

$$k_p' = (p+1)D_M^S \tag{2.30}$$

Combining equations (2.29) and (2.30) yields:

$$x = \sqrt{2(p+1)D_M^S} \tag{2.31}$$

Note if $p=0$ and the concentration of vacancies at the interface is zero, and if γ is unity, then equation (2.27) is equivalent to equation (2.31).

The theory of Wagner matches well with experimental measurements for the oxidation of many metals including,for example, copper and cobalt. It has found wide use to explain experimental phenomena that is limited by diffusion through a growing barrier. Fromhold has found that the parabolic growth law holds under conditions more extensive than those investigated by Wagner.[19] If the diffusion coefficients of the diffusing species do not follow a simple form, or if the conditions at the surface or interface are complicated it is often not possible to find an analytic solution for the growth of the oxide layer. In these cases numerical methods of computation are the most appropriate.[20]

2.3 Fitting Rate of Oxidation Data

In the last section the parabolic growth law (equations (2.27) and (2.31)) was developed for a layer with set concentrations of the diffusing species at its two sides, and with a diffusion coefficient that was not a function of concentration. Experimentally the growth of oxides are often found to follow the parabolic growth law.

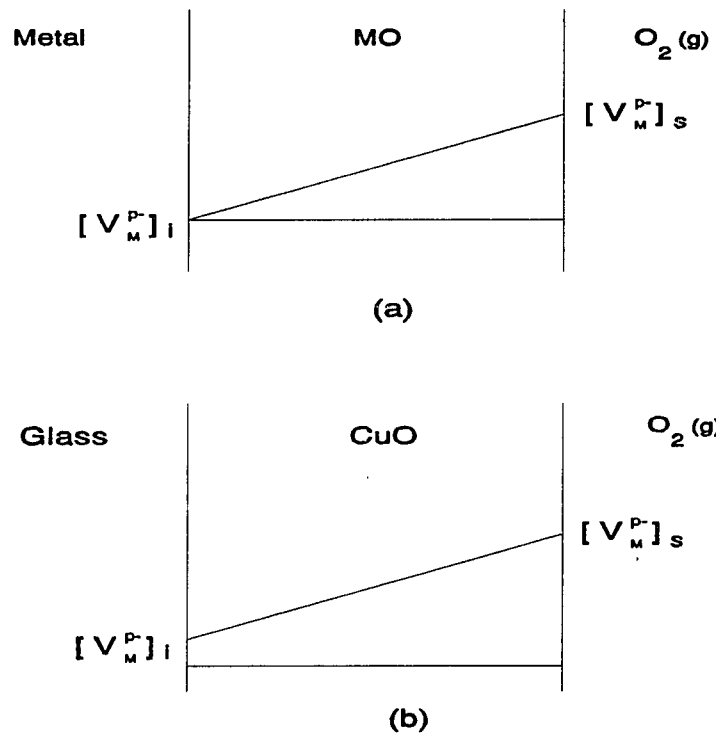

Figure 2.2 Schematic of vacancy concentrations across oxide layer formed on (a) metal and (b) glass.

In the following a method is given for fitting experimental data to the parabolic growth law using a least squares fit. The parabolic growth equation is:

$$w = \sqrt{2kDt} \qquad .32)$$

where w is the width of the film, k is a constant that depends on the concentration of the diffusing species on the inner and outer surface (for the case of neutral vacancies it is developed in appendix B), D is the diffusion coefficient of the diffusing species, and t is the time for growth. Substitution into the equation of parabolic growth a temperature dependent diffusion coefficient of the form:

$$D = D_0 e^{\left(\frac{-Q}{RT}\right)} \qquad (2.33)$$

yields the equation:

$$w = \left(2kD_0 t\right)^{\frac{1}{2}} e^{\left(-\frac{Q}{2RT}\right)} \qquad (2.34)$$

If the log of each side is taken the result is the linear form:

$$\ln w = \ln\sqrt{t} + \ln\sqrt{2kD_0} + \frac{-Q}{2RT} \qquad (2.35)$$

A least squares fit can be used to fit experimental data to this formula. This involves minimizing the function:

$$\sum_{i=1}^{n}\left(\ln\frac{w_i}{\sqrt{t_i}} + \ln\sqrt{2kD_0} + \frac{Q}{2RT_i}\right)^2 \tag{2.36}$$

where T_i, t_i, and y_i are experimentally determined temperatures, times and thicknesses respectfully. Making the following substitutions:

$$y_i = \ln\frac{w_i}{\sqrt{k}} \quad a = \ln\sqrt{kD_0} \quad b = -\frac{Q}{2R} \quad x_i = \frac{1}{T_i} \tag{2.37}$$

equation (2.36) is transformed to:

$$\sum_{i=1}^{n}(y_i - a - bx_i)^2 \tag{2.38}$$

This equation is in standard form for a linear least squares fit. One can determine the values for a and b (if they are not known) which have the best least squares fit, and there relative confidence levels. If the relative error of the data points is known, a number can be also found for the goodness of fit of the proposed model. A discussion of least squares fitting and confidence levels is given in the book Numerical Recipes in C.[21]

2.4 The Effect of the Structure of the Oxide Layer on Oxidation Kinetics

It was previously mentioned that the assumptions of the model were limited since there was also diffusion in the glass. However, a much more fundamental

problem with the solution is that it ignores the structural state of the oxide layer. During the growth of an oxide layer stress build up in the oxide. These stresses can affect the rate of diffusion through the oxide layer. Ultimately something more drastic can occur; the stresses induced in the oxide layer during growth can cause rupture of the film. In oxide films it is usually found the stress increases with thickness of the oxide film.[22] The rate of oxidation of such structures is often found to have a region of parabolic growth as long as the structure remains intact, and changing to a linear relation after the structure begins to rupture,[23] since rupture allows for new avenues of diffusion.

CHAPTER 3

ADHESION OF CuO AND Cu FILMS FORMED ON COPPER ALUMINOSILICATE GLASS

Thin films are applied to bulk materials to produce desired changes in their surface properties. Glass has served both as a coating and as a substrate to which films are applied. Glass glazes have been applied to metal and porcelain surfaces for decoration and for protection. Glass containers are often given a transparent oxide coating to increase their toughness for machine handling.[24] However one impediment to the use of thin films to alter the surface properties of a substrate is the limited adherence of the coating to the substrate. The forces that hold the substrate and the film together, including valence forces (such as van der Waals's and electrostatic) and interlocking forces, are insufficient to keep the film/substrate structure intact. [25]

Due to its high electrical and thermal conductivity, copper has found industrial as a metallization layer for glass. However, the adherence of copper to a glass or ceramic substrate has been found to be poor due to the limited reactivity of copper with oxides.[9] There is therefore interest in increasing the adherence of copper to a glass or ceramic substrate. In the next section of this chapter, the structures found at the substrate/film interface are categorized.[24] A brief description of the mechanisms of failure is then given. The third section is devoted to describing tests for measuring adhesion, including the direct pull-off, peel, and scratch adhesion tests. Though these tests do not directly measure the theoretical adhesion forces described

in the first section, they are found to be of great practical value. The final section describes methods for increasing the adherence of a film of copper to a glass or ceramic substrate.

3.1 Types of Adhesion

The types of bonds that form between a film and the substrate depends on the structure of the interface between the two materials. If the interface is planer and the two materials do not chemically react or intermix then there is a change of energy associated with bringing the two materials together given by:

$$E_{ad} = E_a + E_b - \gamma_{interface} \tag{4.1}$$

where E_a and E_b are the energies of the surface of the substrate and the film respectively, and γ is the interfacial free energy. The energy of adhesion can be small for metal-ceramic systems. However, in general the substrate and film do react, and the interface is not exactly planar. The film can be mechanically anchored in the substrate, chemically reacted with the substrate, or diffusively mixed. Figure 3.1 is a schematic representation of different interface structures. The mechanical interfacial layer forms on rough or porous substrates, creating a mechanical anchor between the substrate and the film. The adhesion depends on the strength of the combination of materials. In the chemical-bonding interfacial layer, a new compound is formed at the interface which is several lattice distances thick. For example, when a glass is coated with a metal, an intermediate oxide layer is

often formed. A diffusional interfacial layer is characterized by a gradual change of the lattice and composition within the film-substrate transition region. It depends on the solubility of the different phases.[24] In the case of a metal bonding with a glass, all three of these mechanisms can be important. They also can be time dependent since further oxidation and diffusion can occur. However a chemically bonding interfacial layer is not normally found between a glass and non-reactive metal such as copper.[9] Mechanical and chemical bonding are influenced by the preparation of the surface. The roughness of the substrate determines the degree of mechanical anchoring. Chemical reactions and diffusion can be hindered by impurities in the substrate. For example, a carbon contamination layer has been shown to detrimentally affect the adhesion of copper to a sapphire substrate.[26]

3.2 Adhesive Failure

Film adhesion can fail if the energy of the internal stresses (which can be relieved through failure) and applied work is greater than the energy of adhesion. However, there is an energy barrier to this process that depends on the deformation of the substrate and film materials, and the mechanism of failure. Failure normally occurs by the initiation and propagation of a crack at the film-substrate interface, but can also be caused by delamination from the free edge or buckling.[27] Internal stresses can arise in the substrate and film due to the deposition process (intrinsic) or thermal stresses due to deposition at elevated temperatures of a film with a different thermal expansion coefficient to that of the substrate.[28,29]

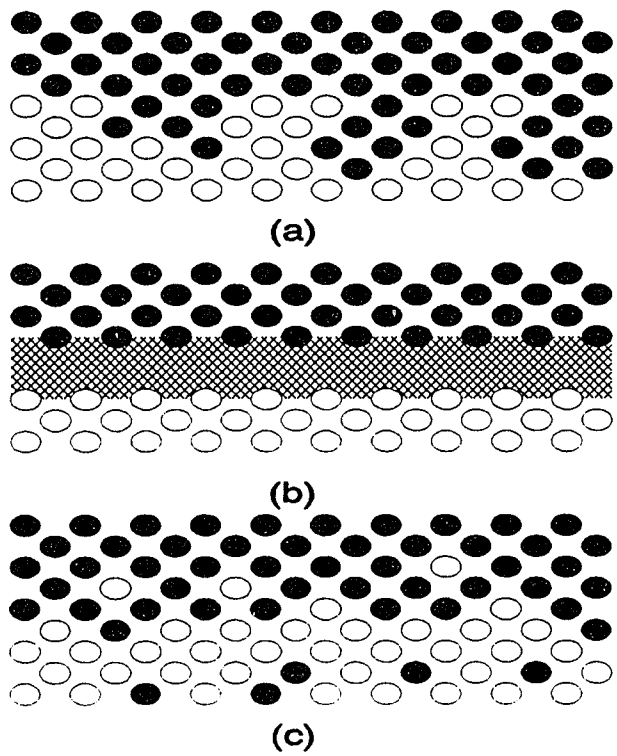

Figure 3.1 (a) mechanical anchoring (b) chemical compound formation (c) diffusion. From Pulkner.[24]

Processes which initiate and propagate cracks at the interface depend on deformation of the film and/or substrate, and therefore depend on the mechanical properties of the materials involved. Models have been developed to describe the initiation of crack propagation. The Barenblatt fracture model predicts failure when the energy stored in the film is sufficient to initiate crack formation:[28]

$$\frac{S^2 t(1-\nu)}{E} > \frac{1}{2}\frac{E_{ad}}{(1+\nu)} \tag{4.2}$$

where ν is the Poisson ratio (about 1/3), S is the internal tensile stress, E is Young's modulus, t the film thickness, and E_{ad} is the energy of adherence of the layers. The expression on the left of the inequality is the stress energy stored in the film. Once cracks have been initiated, their propagation can be curtailed due to the interface geometry.[28] Computational simulations can be used to calculate internal stress in a film and substrate in order to predict failure. Lambropoulos and Wan[27] used finite-element techniques to calculate the stress concentrations near the interface of a single-crystalline film which is bonded to a stiff substrate.

3.3 Adhesion Measurement

There are several tests for measuring adhesion, including nucleation and mechanical tests. In the nucleation methods nucleation theory is used to calculate the adsorption energy of an atom to the substrate from microscopic observation of nucleation together with a description of the deposition system. These nucleation

tests provide direct evidence of the energy of adhesion associated with a film grown on a substrate. In mechanical tests, work is done to separate the film from the substrate. This work includes not only the energy of adhesion, but the work required to deform the substrate and film layer. Although mechanical tests do not measure the energy of adhesion directly, they are useful since they predict how well the structure will survive under differing stresses. The following will briefly describe four mechanical tests: threshold tests, direct pull-off, peel, and scratch adhesion tests.[28] For all the mechanical tests it is important to investigate the structure after the test to determine if the substrate/film interface was the source of failure in order to properly interpret the results of the test. In order to increase the robustness of the structure it is necessary to identify the mode of failure.

Threshold tests involve subjecting the film to stress, and noting whether the structure survives intact. In one test adhesive tape is evenly applied to the film. The tape is then pulled off normal to the substrate. If the film is pulled from the substrate, the force of adhesion between the tape and film is assumed to be greater than the adhesion between the film and the substrate. The reproducibility of this test is variable and is influenced by surface impurities.

Adhesion pull-off tests involve applying a force normal to the interface to separate the film and the substrate. Schematic diagrams of the electromagnetic pull test and the mechanical pull test are given in Figure 3.2.[30] The magnetic pull test involves a nonmagnetic electrically conductive surface layer, and a non-conducting substrate. A conductive pathway is etched in the surface layer. The sample is then

placed in a magnetic field. The current through the conducting film is then increased until the force created by the current in the magnetic field, IxB, is sufficient to pull the layer away from the substrate.

In the direct pull-off test the substrate is cemented on the substrate side and the film side (see Figure 3.2). The structure is subjected to an increasing force until it breaks. If the structure breaks near the film/substrate interface the force at which breakage is assumed to be related to the force of adhesion.

Schematics diagrams of the peel test and the scratch test are given in Figure 3.3. In the peel test, the force registered at the load cell is recorded while the surface layer is pulled from the substrate at a slow uniform speed. In order to prepare samples for the peel test, the thickness of the coating is often increased to approximately 10 μm. In the scratch test, a loaded tip is drawn across a film, and the groove examined with a microscope. The load is increased until it is noted that the film is detaching from the substrate.

It is apparent from the above discussion that pull tests are not the preferred method of adhesion measurement from a theoretical standpoint. However, many of the other methods pose practical problems that limit there use. For example in the peel test one needs a thick film which can be pulled from the substrate. As previously mentioned this can be achieved by thickening the film using evaporation or sputtering. But this alters the structure to be tested. If the material to be tested was composed of a cracked metal layer upon a substrate, the cracks in the metal would be fused with additional metal, giving a new strength to the substrate.

3.4 Increasing Copper/Glass Adhesion

The adhesive strength of the interface between a copper layer and a glass substrate can be increased by varying the chemistry and structure of the interface. The mechanical strength of the structure can be increased by changing the morphology of the structure, for example, by surface roughening. The adhesion of the film can be increased by changing the chemistry of interaction between the film and the substrate by making chemical additions to the film. The technique of ion-beam mixing can be applied to a film that has already formed to increase both mechanical and chemical adhesion. The possibility of applying these different techniques to the formation of a CuO layer on CuAS glass is discussed below.

The strength of the substrate/film structure can be increased by changing the morphology and effective strength of the substrate material. The adherence of the copper to the glass can be increased by roughening the surface and creating a stronger mechanical bond. If the glass is roughened before the creation of the oxide layer, the interface between the glass and the cupric oxide layer will also be rough. When this layer is reduced to copper, the copper will be physically bound to the glass substrate, which can significantly increase adherence. Also, as mentioned in the previous section, surface roughening can hinder crack propagation. Two different methods that are used primarily for roughening a surface are etching and grinding. An abrasive will tend to make grooves in the substrate in the direction of the grinding; the size of the grooves is controlled by the grit used.

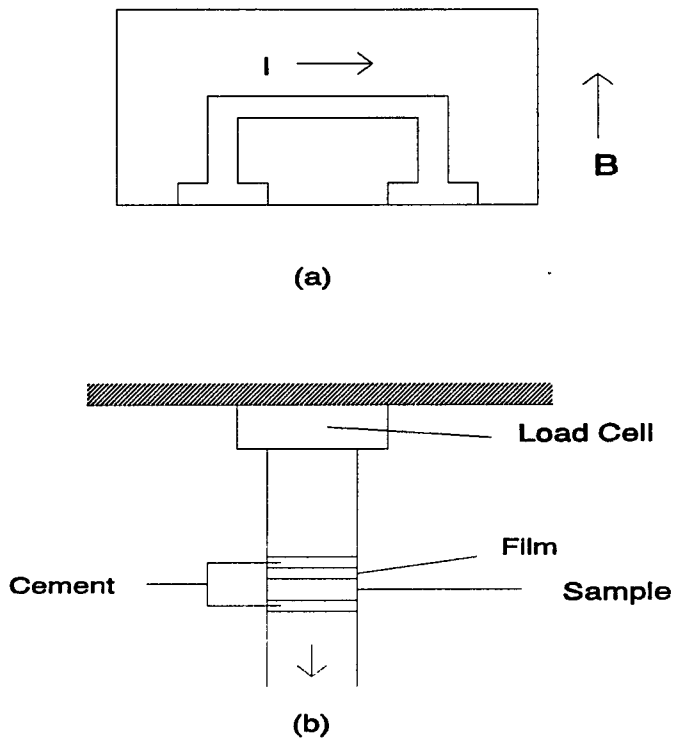

Figure 3.2 (a) Electromagnetic field test. (b) Pull test using load cell.

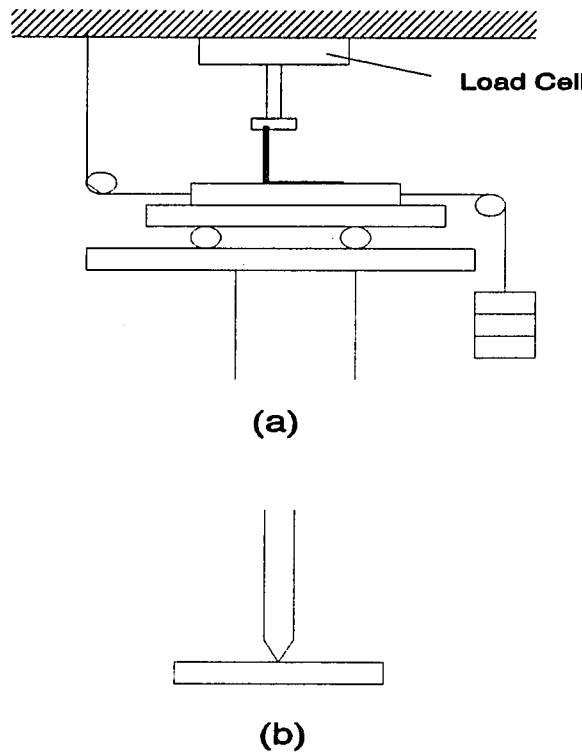

Figure 3.3 (a) Self-aligning peel test (b) Scratch test.

Etching can produce many different surface morphologies. A desirable property of the etch is the ability to produce bell shaped holes so that the top layer is "locked into" the substrate.

Copper does not interact strongly with a glass and therefore has limited chemical adhesion. One method employed to increase adhesion between a non-reactive metal and glass is to add a more reactive intermediate layer. Chromium, for example, will adhere well to glass due to formation of oxides and can be used as an intermediate layer between gold and glass. [24] This has been verified by XPS studies which show that reactive metals, such as chromium, undergo a chemical reaction with the substrate, while non-reactive metals such as Au and Cu do not.[9] In a study by Bortz and Ohuchi, copper was deposited onto both crystalline and amorphous cordierite ($2MgO{\cdot}2Al_2O_3{\cdot}5SiO_2$) based ceramic substrates. Through X-ray Photoelectron Spectroscopy (XPS) the interaction between the copper and the substrate was found to be very weak. The reactive metal titanium, however, was found to be highly react with the cordierite substrate. They suggested the reactive titanium could be used as an intermediate layer between the copper and cordierite based substrate in order to enhance adhesion.[31]

In order to increase the interaction between a metallic film and a glass or ceramic substrate, ion beams have been used to mix the film and substrate material.[26,32] In this technique, the surface of the structure is bombarded with energetic ions. These energetic ions displace atoms in the structure through nuclear and electronic collisions. Collisions near the metal-ceramic interface produce

displacements of the atoms near the interface, mechanically mixing the region near the interface. This technique has been applied to copper-ceramic systems and found to improve the adhesion.[26]

CHAPTER 4

EXPERIMENTAL

The steps involved in producing copper/CuAS glass structures include production of the glass, oxidation of the glass to produce a cupric oxide layer, and reduction of the cupric oxide layer to copper. This chapter on experimental methods includes the procedures used for each of the processing steps, and the methods used for evaluating the resultant structures.

4.1 Method of Glass Production and Evaluation

The admixtures used for producing copper aluminosilicate glasses a-f are listed in Table 4.1. The Cu_2O (98% purity), Al_2O_3 (99.6% purity), SiO_2 (99% purity) and K_2O_3 (99^+% purity) were from Aldrich Chemical Company. The NiO and $NaCO_3$ were from the Johnson Matthey company, with catalog numbers of 87032 and 307528 respectively. The CaO was from Alfa products with a catalog number of 304243. The Cr_2O_3 was also from Alfa products with a purity of 99^+% pure on a metals basis. The admixtures for producing a glasses a and b were mixed by shaking for 15 minutes using a Spectromill Ball Pestle Impact Grinder Model 1100-II (Chemplex Industries Inc. Tuchahoe NY). Glasses *e*, *f*, and *g* were made by mixing an addition to the base powder, *a*, using a spatula. The other powders were mixed by repeated division using a spatula. The powders were packed into an alumina crucible of 10 ml except in the cases of *a*, *b* and *e* where the sizes were 50 ml, 50 ml and 20 ml respectively. After the crucibles were packed they were heated in an electric furnace to the temperature

listed in Table 4.1 for two and one-half hours. The crucibles were then removed from the furnace and air cooled. Glasses of composition *b*, *d*, and *e* were not cooled in the crucible but poured onto a copper plate.

Table 4.1 Composition of Glasses Formed

No.	Composition by mole fraction	Temperature of Melt
a	SiO_2 75 Al_2O_3 12.5 Cu_2O 12.5	1550°C
b	SiO_2 55 Al_2O_3 15 Cu_2O 15 NiO 15	1520°C
c	SiO_2 55 Al_2O_3 15 Cu_2O 15 SnO 15	1420°C
d	SiO_2 55 Al_2O_3 10 Cu_2O 15 K_2O_3 20	1420°C
e	SiO_2 75 Al_2O_3 12.5 Cu_2O 12.5 Cr_2O_3 3	1520°C
f	SiO_2 75 Al_2O_3 12.5 Cu_2O 12.5 CaO 10	1520°C
g	SiO_2 75 Al_2O_3 12.5 Cu_2O 12.5 Na_2O 3	1520°C

The composition of glass *a* relative to the distance from the crucible wall was measured using a Jeol (Model JSM 840A) SEM in EDAX mode. Scans were also taken across the glass crucible interface and through the bulk of the glass. The composition of the glass was measured at 25 points at equal intervals in a linescan of 100 μm. The composition was also taken at 13 points for a scan of approxiamately 4mm.

An electron spectroscopy for chemical analysis (ESCA) scan was made using a $Cu_2O{\cdot}Al_2O_3{\cdot}6SiO2$ glass sample. The machine used was manufactured by Vacuum Generators Scientific Ltd. (Model ESCALAB Mark III).

A differential thermal analysis (DTA) scan was made using 1-1-6 CuAS glass (composition *a*) powder using a Dupont Model 1600 DTA. The CuAS glass was pulverized in the Spectromill Ball Pestle Grinder using a stainless steel pestle and ball, and then pressed into an alumina cup. The run was made from 700°C to 1400°C at a ramp rate of 10°C per minute. The atmosphere used above the sample was air.

4.2 Glass Oxidation and Cupric Oxide Thickness Measurements

An experiment was designed to measure the oxidation of the Cu_2O-Al_2O_3-$6SiO_2$ glass in air at 460, 480 and 500°C. Glass which was cooled in the crucible was cut into slabs of roughly 4 mm thickness. Two different methods were used to produce glass slabs of approxiamate dimensions 4 mm by 2 mm by 1 cm with one of the side faces polished. In the first method the 4 mm slabs were polished using the schedule in Table 4.2, and then cut to proper dimensions using a diamond saw. In the second method the samples were cut to approxiamately 4 mm by 2 mm by 1 cm and then mounted to a cast iron platten. The samples were then ground with a 15 μm alumina slurry on a R. Howard Strasburgh Inc. model 6BK-16 inch Ring Precision Polishmaster. The platten was then cleaned and transferred to another model 6BK-16 inch using a a 1 μm cerium oxide slurry with a Pellon Pad Polishing Cloth. After the polishing the glass was washed with soap and a solvent to remove oil from the surface. The glass was then put in the receptor shown in Figure 4.1 with the polished surface up. A type B thermocouple was placed up into the end of the

receptor to measure the temperature (the error of not using a cold junction compensator being only 1°C in temperature range of interest). A tube furnace with a type k thermocouple for control was used and adjusted until the reading at the type B thermocouple was at the desired value (Figure 4.1). A sample was then placed in the holder. A small pump was used to created a flow of air through the drierite column and through the quartz tube which contained the sample. Samples were also oxidized for subsequent reduction. When the oxidation time was 15 minutes or less the furnace tube was flushed with UHP N_2 until the sample reached the desired oxidation temperature (approximately 10 minutes), and then the gas was switched back to air dried by the drierite column.

Table 4.2 Polishing schedule for copper aluminosilicate glass.

Paper/Cloth/Abrasive	Time
Silicon Carbide 120	until epoxy removed from surface
Silicon Carbide 320	2 minutes
Chemomet with 6μ diamond suspension	6 minutes
Chemomet with Mastermet	8 minutes

After the pieces were oxidized they were placed in epoxy with the polished side perpendicular to the surface. The pieces were then polished as before and coated with carbon. The SEM was used to measure the thickness of the layer.

An alternate procedure was used to measure the thickness of the oxide layer for glass samples. The pieces of glass were oxidized using the procedure described above. Then a layer of wax was melted onto part of the oxide layer. The piece of glass was then immersed in 1 part 16N HCl to 2 parts deionized H_2O. The sample was kept in the acid bath for ten minutes, slightly stirring the solution. The sample was then removed from the solution and washed with deionized water. After washing the sample the wax was removed by dissolving it in CCl_4. The oxide remained where the wax had been. Its thickness was measured by using a surface profiler across the edge of the oxide film. The surface profiler used was a DEKTAK IIA (Sloan Technology Corporation) with a 12.5 μm radius stylus.

4.3 Production of Glass/Copper Structures

For reduction experiments both oxidize samples of varying surface roughnesses and times of oxidation were used. The CuAS glass samples were reduced by heating in 3% H_2 97% N_2 at one atmosphere at 450°C - 500°C using the apparatus used to oxidize samples.

Samples of CuAS glass of varying roughness 1 cm x 1 cm x 0.2 cm were cut, polished and oxidized following the procedure used for the samples used in the oxidation study. The cupric oxide layers were then reduced using a mixture of 3% H_2 and 97% N_2.

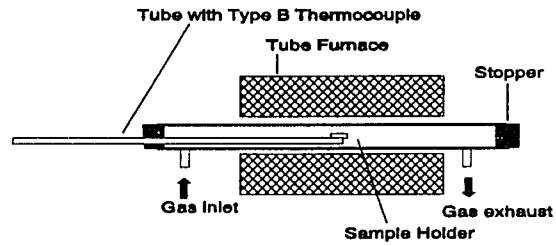

(a)

(b)

Figure 4.1 (a) Furnace used for oxidation and reduction of glass samples. (b) Alumina tube sample holder with tip of type b thermocouple under sample.

4.4 Measurement of Copper Adhesion to Glass

The structures which were produced according to differing parameters were subjected to a pull test to evaluate the adherence of the copper to the glass. The testing method was a pull test similar to the mechanical pull test described in Chapter 4. However cement was not used. Instead on one side a wax was used to mount the sample. On the other side double sided sticky tape was used between the specimen and the pull testing machine. An Ingstron machine was used to monitor the force as the structure was slowly pulled apart giving a strain force curve for the breaking apart of the structure. A 2 kg load cell was used, which was calibrated with a 100 g weight at the beginning of each set of experiments. Before the pull was begun, the tape and sample were compressed together with a force of 1 kg, and then released back to zero force. The pull rate used was .02 inches a minute with a chart speed of 2 inches a minute. In each case the structure of the interface was investigated after the pull was performed.

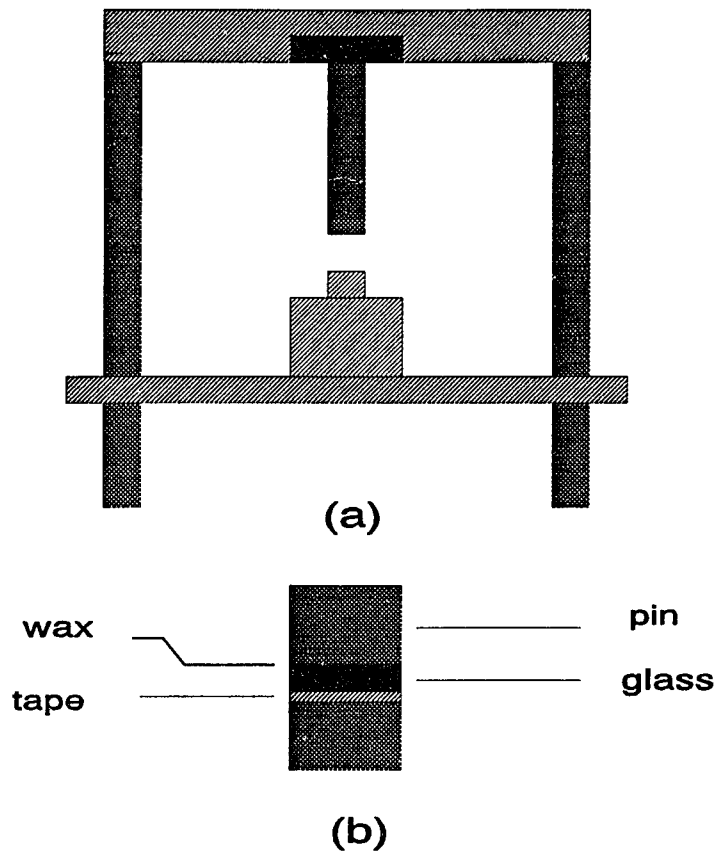

Figure 4.2 (a) Ingstron with sample loaded. Bottom shaded region is table which moves up and down. (b) close up of sample.

CHAPTER 5

RESULTS

The results are divided into four sections. The first contains experimental results concerning the use of an alumina crucible to melt copper aluminosilicate glass. Results for oxidation of CuAS glass in air follow in the next section. The final section contains data on the formation of copper layers on copper aluminosilicate glass and their adherence to the glass.

5.1 Glass Produced in Alumina Crucible

The glasses produced (Table 4.1) were found to be predominately dark brown in color with notable exceptions of glasses *c* and *e*. The bulk of glass *e* was dark brown, but it had an additional green phase. Glass *c* was straw colored, though the glass was not homogeneous due to the incomplete mixing of the tin.

Tables 5.1 and 5.2 give the composition of the measured across the crucible-$Cu_2O{\cdot}Al_2O_3{\cdot}6SiO_2$ glass interface by an SEM EDAX scan. The scan for Table 5.1 consisted of 25 points across a distance of 100 μm, while the scan for Table 5.2 consisted of 13 points across a distance of approximately 4 mm.

Figure 5.1 is an X-ray photoelectron spectroscopy scan for the binding energy of electrons to the copper aluminosilicate glass formed at 1520°C in an alumina crucible.[33]

Kamiya *et al.* found the ratio of copper in the cuprous state to total copper to be approximately 0.9 for 1-1-4 CuAS glass melted near 1500°C.[7] Modeling the glass as an ideal mixture of components (equations (2.1) - (2.6)), the free energy of formation of 4 moles of cupric oxide from 2 moles of cuprous oxide and 1 mole of oxygen at 0.2 atmospheres is found to be 121 kJ at 1500°C. Assuming the free energy change for the reaction is a linear function of temperature from 1100°C to 1700°C the free energy change for the reaction is:

$$\Delta G = 121{,}000 - (1773 - T)290 \; Joules$$

Using equation 2.6 (which assumes ideal solution behavoir) and equation (5.12) the ratio of the molar concentration of the cuprous ion to the molar concentration of the total copper ions can be found as was described in Chapter 2. Table 5.3 gives the results of these calculations. The table relates the temperature of the melt to the expected equilibrium constant K_{eq} and to the calculated ratio of the cuprous to cupric oxide.

A DTA scan for the 1-1-6 CuAS glass is presented in Figure 5.2. The run was made from 700°C to 1400°C at a ramp rate of 10°C per minute with the glass powder pressed in an alumina cup. The atmosphere used above the sample was air. There is an exothermic peak at 929°C and an endothermic peak at 987°C.

Table 5.1 Atomic percent of metal ions found in 100μm scan across alumina crucible/$Cu_2O{\cdot}Al_2O{\cdot}6SiO_2$ glass interface.

Distance along scan (μm) scan	Atomic Percent Al	Atomic Percent Si	Atomic Percent Cu
0.0	100.00	0.00	0.00
4.17	99.19	0.81	0.00
8.33	98.65	0.00	1.35
12.5	73.18	20.36	5.84
16.67	23.14	52.18	24.68
20.83	82.72	13.93	3.35
25.00	88.93	8.44	2.63
29.17	100.00	0.00	0.00
33.30	100.00	0.00	0.00
37.50	99.20	0.80	0.00
41.67	98.85	1.15	0.00
45.83	98.81	0.00	1.19
50.00	84.59	15.41	0.00
54.17	69.50	28.77	1.73
58.33	69.18	28.93	1.90
62.50	63.58	34.23	2.19
66.67	35.09	54.74	10.16
70.83	22.77	58.28	18.95
75.00	65.34	33.37	1.29
79.17	24.83	55.37	19.80
83.33	24.29	55.15	20.56
87.50	23.60	53.44	22.96
91.67	26.28	53.97	19.75
95.83	26.58	51.54	21.88
100.00	26.77	52.89	20.34

Table 5.2 Atomic percent of metal ions found in ~4 mm scan across alumina crucible/$Cu_2O \cdot Al_2O \cdot 6SiO_2$ glass interface.

Distance along Scan (mm)	Atomic Percent Al	Atomic Percent Si	Atomic percent Cu
-1.679	99.42	0.00	0.58
-1.246	99.29	0.71	0.00
-0.822	98.32	0.87	0.81
-0.406	100.00	0.00	0.00
0.00	25.44	54.45	20.11
0.394	20.90	61.63	17.47
.773	19.90	61.77	18.33
1.136	19.77	61.34	18.89
1.479	19.40	60.71	19.90
1.799	19.49	61.51	18.99
2.092	19.39	61.90	18.71
2.352	19.53	61.65	18.83
2.576	19.09	60.36	20.55

Table 5.3 Calculation of ratio of cuprous to total copper content in 1-1-6 CuAS glass assuming ideal activities.

Temperature °C	$K_{eq} \cdot PO_2$	$[Cu^+]/[Cu^{++}] + [Cu^+]$
1200	$1.3033 \cdot 10^{-2}$	.670
1250	$4.5438 \cdot 10^{-3}$	.734
1300	$1.6938 \cdot 10^{-3}$	.784
1350	$6.7096 \cdot 10^{-4}$	.824
1400	$2.8092 \cdot 10^{-4}$	.855
1450	$1.2371 \cdot 10^{-4}$	.880
1500	$5.7057 \cdot 10^{-5}$	.900
1550	$2.7457 \cdot 10^{-5}$	.916
1600	$1.3739 \cdot 10^{-5}$	.929
1650	$7.1268 \cdot 10^{-6}$	.939
1700	$3.8219 \cdot 10^{-6}$	.948

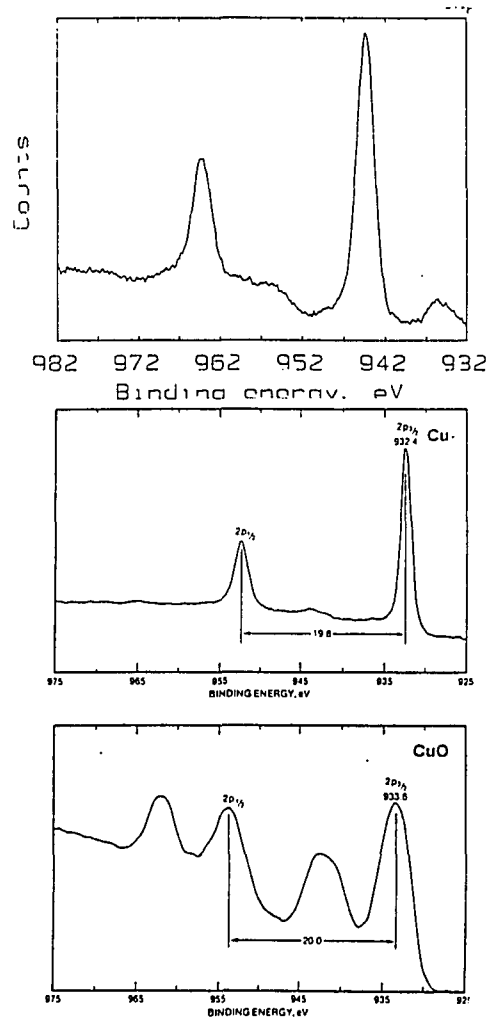

Figure 5.1 XPS of copper alumina glass melted and cooled in an alumina crucible. Data for comparison is taken from *Handbook of X-ray Photoelectron Spectroscopy*, C.D. Wagner *et al.*[33]

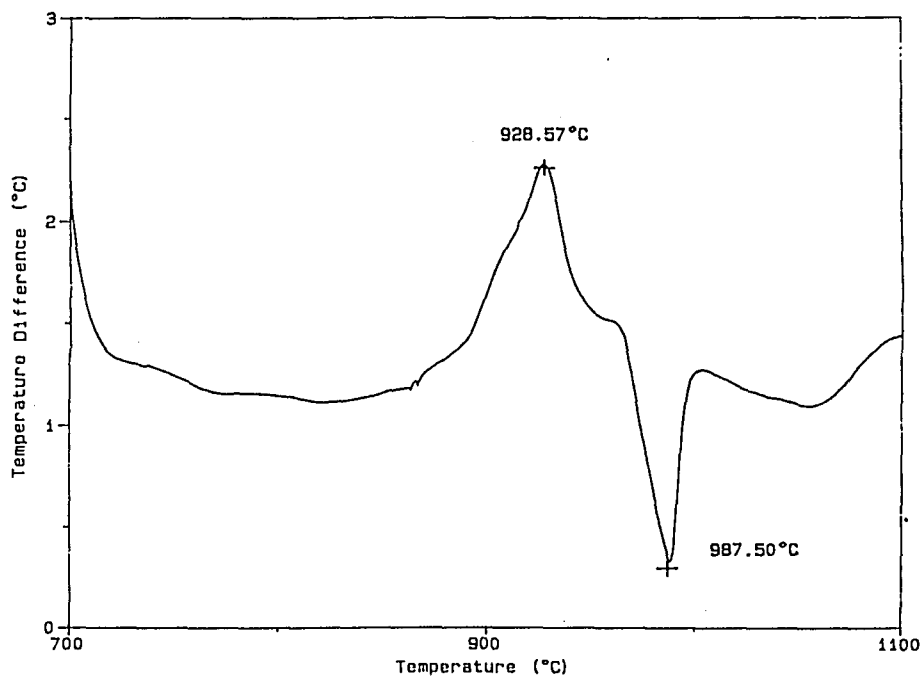

Figure 5.2 DTA scan for $Cu_2O{\cdot}Al_2O_3{\cdot}6SiO_2$ glass.

5.2 Oxidation of CuAS Glass

The glass was oxidized at 460°C, 480°C and 500°C in dry air. The oxidation temperature, oxidation time, and thickness of the oxide layer as measured by SEM, are given in Table 5.4. The entries with an asterisk were measured with the DEKTAK surface profile, and therefore average heights would not correspond to average heights for SEM pictures. Figure 5.3 is shows a typical SEM micrograph that was used to calculate the thickness of the oxide layer.

The results for Dektak traces of two glass samples which were oxidized for one hour at 500°C are given in Figure 5.4.

5.3 Processing of CuAS Glass with Additional Oxides

Table 4.1 gives the compositions of glasses produced for the processing study. All were cooled in a crucible except for compositions *b* and *d* which were poured. All samples were oxidized and reduced according to the procedure in the experimental section. The electrical conductivity of the layer produced on the surface was checked using an ohmmeter. Samples *a*, *b*, *c*, *e*, *f* and *g* all showed resistances less than 2 ohms for pieces roughly 0.5 cm by 0.5 cm. Samples *d* had resistances greater than a 10^6 ohms for pieces roughly 0.5 cm by 0.5 cm. It is also noted that when the glass with nickel oxide was formed in the alumina crucible there was less cracking upon cooling.

Table 5.4 Cupric oxide layer thickness on copper aluminosilicate glass as a function of oxidation temperature and time.

Oxidation Temperature °C	Oxidation Time (hours)	Peak Thickness (μm)	Average Thickness (μm)
460	4	1.46	*
460	24	3.86	3.0
460	48	4.12	3.5
460	72	5.1	4.6
480	4	1.6	*
480	24	4.6	4.1
480	48	6.12	5.4
480	72	7.64	6.6
500	0.5	0.87	0.75
500	1	1.34	*
500	2	1.82	1.45
500	4	2.16	1.85
500	6	2.82	2.64
500	10	3.35	3.09
500	16	4.15	3.65

* measured by surface profile method, no average comparable to average of SEM measurements.

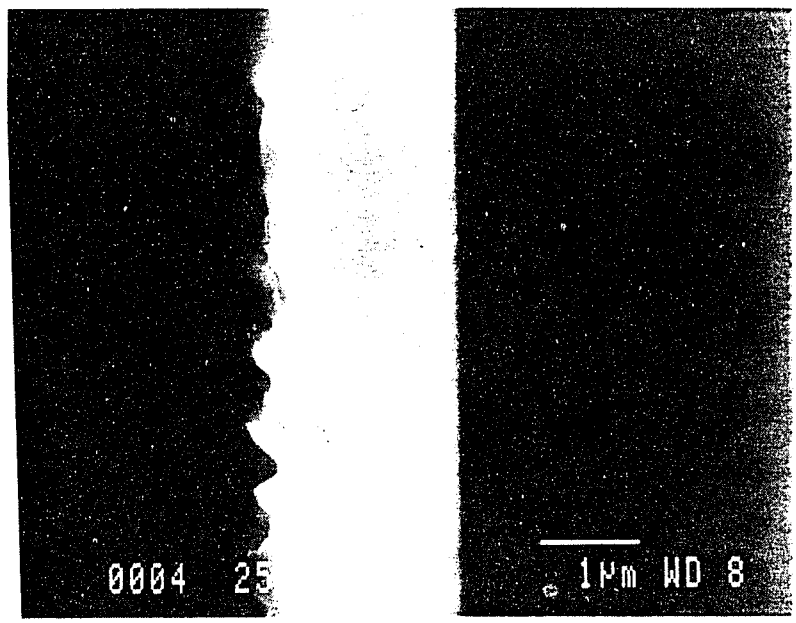

Figure 5.3 Example of the oxide layer formed on $Cu_2O{\cdot}Al_2O_3{\cdot}6SiO_2$ glass after oxidation in air. This sample was oxidized for 4 hours at 500°C.

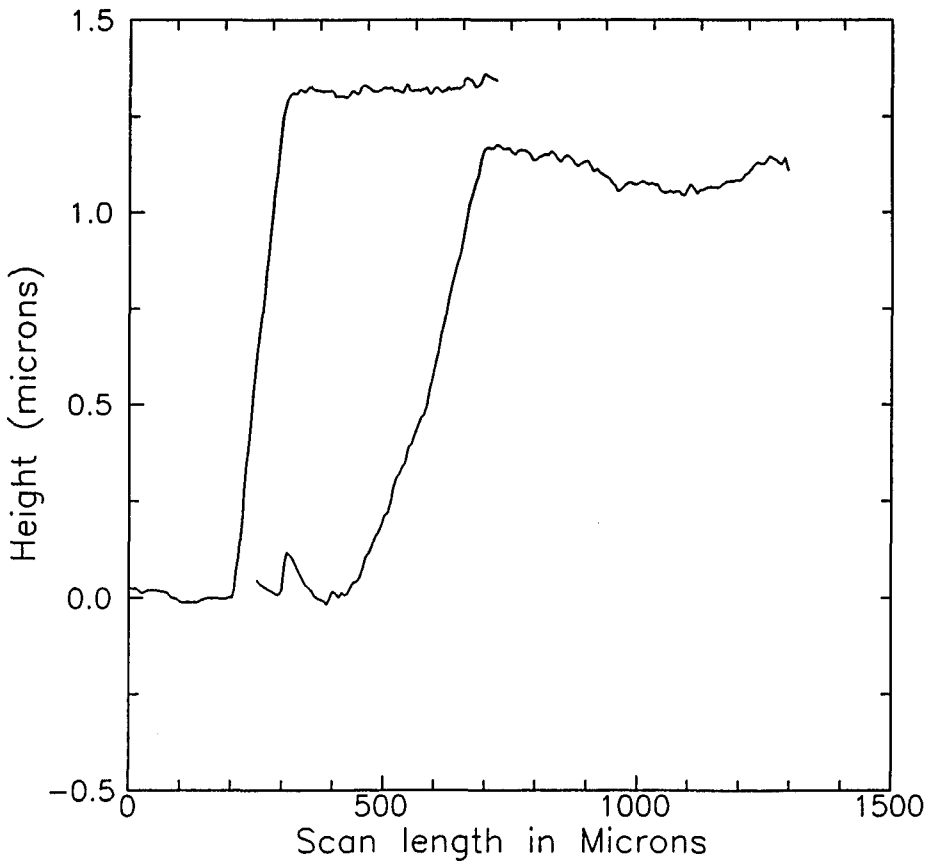

Figure 5.4 Surface profile across edge of oxide film of samples oxidized in air at 500°C for one hour. The sample on the left was not annealed. The sample on the right was annealed at 800°C.

5.4 Characterization of Copper Layers formed on Copper Aluminosilicate Glass

The cupric oxide layers formed on CuAS glass were reduced to copper using a gas mixture of 97% N_2 and 3% H_2. The copper layers formed retained the cracks observed in the cupric oxide layer. When the copper was formed on a smooth surface the copper peeled up at the crack edges. Holes were observed in copper layers formed on rough glass surfaces.

Measurements were made of the adhesion of copper films to the copper aluminosilicate glass. The results for the tape pull test measurements are given in Tables 5.5 to 5.36 were the force is given in terms of grams force, and the displacement is given in inches. The data is plotted in terms of pull stress (force divided by area of sample) in Figures 5.7 to 5.13.

Table 5.5 Pull test force (grams) versus displacement (inches) for removal of tape from CuAS glass.
Sample Number: 1 Sample Area: 0.956 cm^2
Maximum Stress: 135 kN/m^2

Displacement (inches)	0.000	0.002	0.004	0.006	0.008
0.00	0	60	120	180	240
0.01	320	400	480	580	660
0.02	740	820	900	980	1040
0.03	1100	1160	1200	1230	1260
0.04	1300	1305	1310	1320	1310
0.05	1310	1310	1310	1290	1270
0.06	1250	1240	1200	1170	1160

Table 5.6 Pull test force (grams) versus displacement (inches) for removal of tape from CuAS glass.
Sample number: 2 Sample area: 0.956 cm^2
Maximum pull stress: 131 kN/m^2

Displacement (inches)	0.000	0.002	0.004	0.006	0.008
0.00	0	40	90	140	180
0.01	220	280	340	410	480
0.02	580	660	740	810	880
0.03	950	1000	1050	1100	1150
0.04	1200	1140	1160	1180	1200
0.05	1210	1230	1260	1270	1280
0.06	1280	1280	1270	1270	1270
0.07	1270	1250	1230	1210	1190
0.08	1150	1140			

Table 5.7 Tape pull test force (grams) versus displacement (inches) for CuAS glass sample 3. Sample 3 was oxidized in air at 400°C for 1 hour, and then reduced with 97% N_2 3% H_2 gas mixture at 400°C for 15 minutes. Tested surface of sample was polished before treatment. 8
Sample No.: 3 Sample Area: 0.857 cm^2
Maximum pull stress: 146 kN/m^2

Displacement (inches)	0.000	0.002	0.004	0.006	0.008
0.00	0	70	160	260	370
0.01	480	600	700	810	900
0.02	980	1050	1120	1170	1220
0.03	1250	1260	1270	1270	1275
0.04	1280	1275	1250	1220	1160
0.05	1120	1090	1040	900	

Table 5.8 Tape pull test force (grams) versus displacement (inches) for CuAS glass sample 4. Sample 4 was oxidized in air at 460°C for 5 minutes, and then reduced with 97% N_2 3% H_2 gas mixture at 460°C for 15 minutes. Tested surface of sample was polished before treatment.
Sample No.: 4 Sample Area: 0.918 cm^2
Maximum pull stress: 154 kN/m^2

Displacement (inches)	0.000	0.002	0.004	0.006	0.008
0.00	0	40	100	150	215
0.01	280	375	455	540	630
0.02	720	800	880	940	1005
0.03	1070	1115	1175	1220	1260
0.04	1300	1340	1370	1400	1420
0.05	1435	1440	1440	1420	1120
0.06	760	430	340	290	250
0.07	230	210	200		

Table 5.9 Tape pull test force (grams) versus displacement (inches) for CuAS glass sample 5. Sample 5 was oxidized in air at 460°C for 15 minutes, and then reduced with 97% N_2 3% H_2 gas mixture at 460°C for 15 minutes. Tested surface of sample was polished before treatment.
Sample No.:5 Sample Area: 0.892 cm^2
Maximum pull stress: 23 kN/m^2

Displacement (inches)	0.000	0.002	0.004	0.006	0.008
0.00	0	50	90	125	160
0.01	185	205	205	205	200
0.02	190	185	170	160	145

Table 5.10 Tape pull test force (grams) versus displacement (inches) for CuAS glass sample 6. Sample 6 was oxidized in air at 460°C for 15 minutes, and then reduced with 97% N_2 3% H_2 gas mixture at 460°C for 15 minutes. Tested surface of sample was polished before treatment.
Sample No.: 6 Sample Area: 0.65 cm^2
Maximum pull stress: 129 kN/m^2

Displacement (inches)	0.000	0.002	0.004	0.006	0.008
0.00	0	60	110	170	230
0.01	300	350	420	485	550
0.02	610	660	710	760	800
0.03	840	860	850	810	810
0.04	810	805	790	760	720
0.05	630	480			

Table 5.11 Tape pull test force (grams) versus displacement (inches) for CuAS glass sample 7. Sample 7 was oxidized in air at 460°C for 15 minutes, and then reduced with 97% N_2 3% H_2 gas mixture at 460°C for 15 minutes. Tested surface of sample was polished before treatment.
Sample No.:7 Sample Area: 1.11 cm^2
Maximum pull stress 65 kN/m^2

Displacement (inches)	0.000	0.002	0.004	0.006	0.008
0.00	0	30	60	90	120
0.01	160	190	230	270	320
0.02	360	420	460	510	560
0.03	590	620	640	670	700
0.04	720	730	740	740	720
0.05	700	670	650	630	580
0.06	520	500			

Table 5.12 Tape pull test force (grams) versus displacement (inches) for CuAS glass sample 8. Sample 8 was oxidized in air at 500°C for 5 minutes, and then reduced with 97% N_2 3% H_2 gas mixture at 500°C for 15 minutes. Tested surface of sample was polished before treatment.
Sample Number: 8 Sample Area: 0.72cm^2
Maximum pull stress: 130 kN/m^2

Displacement (inches)	0.000	0.002	0.004	0.006	0.008
0.00	0	40	70	110	150
0.01	190	230	280	320	365
0.02	405	450	490	510	550
0.03	585	620	660	690	720
0.04	750	780	805	835	860
0.05	880	910	930	925	930
0.06	940	950	955	936	910
0.07	870	800	710	600	420
0.08	60				

Table 5.13 Tape pull test force (grams) versus displacement (inches) for CuAS glass sample 9. Sample 9 was oxidized in air at 500°C for 15 minutes, and then reduced with 97% N_2 3% H_2 gas mixture at 500°C for 15 minutes. Tested surface of sample was polished before treatment.
Sample Number: 9 Sample Area: 0.67cm^2
Maximum pull stress: 93 kN/m^2

Displacement (inches)	0.000	0.002	0.004	0.006	0.008
0.00	0	30	60	100	140
0.01	180	240	280	340	380
0.02	430	480	520	550	570
0.03	585	605	620	635	630
0.04	620	600	550	540	530
0.05	510	490	490	450	410

Table 5.14 Tape pull test force (grams) versus displacement (inches) for CuAS glass sample 10. Sample 10 was oxidized in air at 500°C for 15 minutes, and then reduced with 97% N_2 3% H_2 gas mixture at 500°C for 15 minutes. Preparation included annealing sample and polishing the surface to be tested.
Sample Number: 10 Sample Area: 0.86 cm^2
Maximum pull stress: 96 kN/m^2

Displacement					
0.00	0	40	80	120	150
0.01	190	230	260	310	350
0.02	400	455	500	545	585
0.03	620	660	680	715	740
0.04	760	775	785	800	815
0.05	825	835	840	845	680
0.06	600	200			

Table 5.15 Tape pull test force (grams) versus displacement (inches) for CuAS glass sample 11. Sample 11 was oxidized in air at 500°C for 30 minutes, and then reduced with 97% N_2 3% H_2 gas mixture at 500°C for 15 minutes. Tested surface of sample was polished before treatment.
Sample Number: 11 Sample Area: 1.11 cm^2
Maximum pull stress: 17 kN/m^2

Displacement (inches)	0.000	0.002	0.004	0.006	0.008
0.00	0	10	50	90	130
0.01	170	190	195	195	195
0.02	180	160	160	160	160
0.03	160	165	170	170	170
0.04	165	165	165	165	165
0.05	160	140	130		

Table 5.16 Tape pull test force (grams) versus displacement (inches) for CuAS glass sample 12. Sample 12 was oxidized in air at 500°C for 30 minutes, and then reduced with 97% N_2 3% H_2 gas mixture at 500°C for 15 minutes. Tested surface of sample was polished before treatment.
Sample Number: 12 Sample Area: 1.08 cm^2
Maximum pull stress: 27 kN/m^2

Displacement (inches)	0.000	0.002	0.004	0.006	0.008
0.00	0	40	90	140	190
0.01	240	280	285	300	300
0.02	290	295	300	300	290
0.03	290	290	290	285	280
0.04	280	280	280	270	260

Table 5.17 Tape pull test force (grams) versus displacement (inches) for CuAS glass sample 13. Sample 13 was oxidized in air at 500°C for 30 minutes, and then reduced with 97% N_2 3% H_2 gas mixture at 500°C for 15 minutes. Tested surface of sample was polished before treatment.
Sample Number: 13 Sample Area: 0.889 cm^2
Maximum pull stress: 25 kN/m^2

Displacement (inches)	0.000	0.002	0.004	0.006	0.008
0.00	0	60	120	180	220
0.01	230	220	230	220	200
0.02	170	160			

Table 5.18 Tape pull test force (grams) versus displacement (inches) for CuAS glass sample 14. Sample 14 was oxidized in air at 500°C for 30 minutes, and then reduced with 97% N_2 3% H_2 gas mixture at 500°C for 15 minutes. Preparation included annealing sample and polishing the surface to be tested.
Sample Number: 14 Sample Area: 0.883 cm^2
Maximum pull stress: 71 kN/m^2

Displacement (inches)	0.000	0.002	0.004	0.006	0.008
0.00	0	50	100	140	200
0.01	260	340	420	500	560
0.02	620	640	640	560	390
0.03	260	200			

Table 5.19 Tape pull test force (grams) versus displacement (inches) for CuAS glass sample 15. Sample 15 was oxidized in air at 500°C for 30 minutes, and then reduced with 97% N_2 3% H_2 gas mixture at 500°C for 15 minutes. Preparation included annealing sample and polishing the surface to be tested.
Sample Number: 15 Sample Area: 0.98 cm^2
Maximum pull stress: 19 kN/m^2

Displacement (inches)	0.000	0.002	0.004	0.006	0.008
0.00	0	40	80	120	150
0.01	180	185	185	180	175
0.02	170	165	160	160	160
0.03	160	160	155	150	150
0.04	135	120	120	105	100
0.05	80				

Table 5.20 Tape pull test force (grams) versus displacement (inches) for CuAS glass sample 16. Sample 16 was oxidized in air at 500°C for 1 hour, and then reduced with 97% N_2 3% H_2 gas mixture at 500°C for 15 minutes. Tested surface of sample was polished before treatment.
Sample Number: 16 Sample Area: 1.06 cm^2
Maximum pull stress: 32 kN/m^2

Displacement (inches)	0.000	0.002	0.004	0.006	0.008
0.00	0	30	75	125	165
0.01	220	260	310	350	330
0.02	310	320	310	310	320
0.03	330	340	350	350	330
0.04	335	335	335	335	300
0.05	300	280			

Table 5.21 Tape pull test force (grams) versus displacement (inches) for CuAS glass sample 17. Sample 17 was oxidized in air at 500°C for 2 hours, and then reduced with 97% N_2 3% H_2 gas mixture at 500°C for 15 minutes. Tested surface of sample was polished before treatment.
Sample Number: 17 Sample Area: 0.955 cm^2
Maximum pull stress: 12 kN/m^2

Displacement (inches)	0.000	0.002	0.004	0.006	0.008
0.00	0	50	85	110	115
0.01	115	115	105	90	80

Table 5.22 Tape pull test force (grams) versus displacement (inches) for CuAS glass sample 18. Sample 18 was oxidized in air at 500°C for 2 hours, and then reduced with 97% N_2 3% H_2 gas mixture at 500°C for 15 minutes. Tested surface of sample was polished before treatment.
Sample Number: 18 Sample Area: 0.96 cm^2
Maximum pull stress: 13 kN/m^2

Displacement (inches)	0.000	0.002	0.004	0.006	0.008
0.00	0	20	35	60	90
0.01	105	110	120	120	125
0.02	120	120	120	120	125
0.03	120	125	125	125	120
0.04	120	120	120	120	120

Table 5.23 Tape pull test force (grams) versus displacement (inches) for CuAS glass sample 19. Sample 19 was oxidized in air at 500°C for 2 hours, and then reduced with 97% N_2 3% H_2 gas mixture at 500°C for 15 minutes. Preparation included annealing sample and polishing the surface to be tested.
Sample Number: 19 Sample Area: 0.88 cm^2
Maximum pull stress: 62 kN/m^2

Displacement (inches)	0.000	0.002	0.004	0.006	0.008
0.00	0	30	60	100	140
0.01	180	220	260	320	360
0.02	410	435	460	480	490
0.03	510	520	535	550	560
0.04	560	560	540	510	420
0.05	385	355	355	300	160
0.06	120	110			

Table 5.24 Tape pull test force (grams) versus displacement (inches) for CuAS glass sample 20. Sample 20 was oxidized in air at 500°C for 2 hours, and then reduced with 97% N_2 3% H_2 gas mixture at 500°C for 15 minutes. Preparation included annealing sample and polishing the surface to be tested.
Sample Number: 20 Sample Area: 0.91 cm^2
Maximum pull stress: 39 kN/m^2

Displacement (inches)	0.000	0.002	0.004	0.006	0.008
0.00	0	20	50	90	130
0.01	160	185	210	240	265
0.02	285	285	300	315	330
0.03	340	345	350	360	270
0.04	270	270	270	260	

Table 5.25 Tape pull test force (grams) versus displacement (inches) for CuAS glass sample 21. Sample 21 was oxidized in air at 500°C for 30 minutes, and then reduced with 97% N_2 3% H_2 gas mixture at 500°C for 15 minutes. Tested surface of sample, and then etched with solution of one part 3N HF, one part deionized H_2O and one part 16N HCl.
Sample Number: 21 Sample Area: 0.86 cm^2
Maximum pull stress: 19 kN/m^2

Displacement (inches)	0.000	0.002	0.004	0.006	0.008
0.00	0	20	35	50	65
0.01	80	100	110	120	130
0.02	140	140	145	155	160
0.03	165	170	170	170	175
0.04	150	140			

Table 5.26 Tape pull test force (grams) versus displacement (inches) for CuAS glass sample 22. Sample 22 was oxidized in air at 500°C for 30 minutes, and then reduced with 97% N_2 3% H_2 gas mixture at 500°C for 15 minutes. Tested surface of sample was polished, and then roughened with 1200 grit SiC paper before treatment.
Sample Number: 22 Sample Area: 0.81 cm^2
Maximum pull stress: 41 kN/m^2

Displacement (inches)	0.000	0.002	0.004	0.006	0.008
0.00	0	40	60	90	115
0.01	140	170	190	220	250
0.02	260	260	250	240	230
0.03	220	230	250	260	270
0.04	275	285	295	305	315
0.05	325	340	220		

Table 5.27 Tape pull test force (grams) versus displacement (inches) for CuAS glass sample 23. Sample 23 was oxidized in air at 500°C for 30 minutes, and then reduced with 97% N_2 3% H_2 gas mixture at 500°C for 15 minutes. Tested surface of sample was polished, and then roughened with 1200 grit SiC paper before treatment.
Sample Number: 23 Sample Area: 0.81 cm^2
Maximum pull stress: 103 kN/m^2

Displacement (inches)	0.000	0.002	0.004	0.006	0.008
0.00	0	30	80	120	180
0.01	235	300	360	430	500
0.02	575	650	715	780	830
0.03	850	795	750	730	700
0.04	645	630	620	600	560

Table 5.28 Tape pull test force (grams) versus displacement (inches) for CuAS glass sample 24. Sample 24 was oxidized in air at 500°C for 30 minutes, and then reduced with 97% N_2 3% H_2 gas mixture at 500°C for 15 minutes. Tested surface of sample was polished, and then roughened with 1200 grit SiC paper before treatment.
Sample Number: 24 Sample Area: 0.94 cm^2
Maximum pull stress: 18 kN/m^2

Displacement (inches)	0.000	0.002	0.004	0.006	0.008
0.00	0	20	40	70	90
0.01	115	120	140	145	155
0.02	160	165	165	170	170
0.03	170	175	175	175	170
0.04	170	170	165	155	145
0.05	120	100	90	65	65

Table 5.29 Tape pull test force (grams) versus displacement (inches) for CuAS glass sample 25. Sample 25 was oxidized in air at 500°C for 30 minutes, and then reduced with 97% N_2 3% H_2 gas mixture at 500°C for 15 minutes. Tested surface of sample was polished, and then roughened with 600 grit SiC paper before treatment.
Sample Number: 25 Sample Area: 0.76 cm^2
Maximum pull stress: 171 kN/m^2
Comment: Copper mostly remained

Displacement (inches)	0.000	0.002	0.004	0.006	0.008
0.00	0	50	100	130	170
0.01	205	245	280	330	370
0.02	420	480	535	590	650
0.03	700	760	810	860	910
0.04	950	995	1040	1070	1110
0.05	1140	1170	1195	1220	1240
0.06	1250	1265	1275	1280	1290
0.07	1310	1315	1320	1325	1325
0.08	1325	1330	1305	1290	1260
0.09	1200	1165	1120	1080	1050
0.10	1010	980			

Table 5.30 Tape pull test force (grams) versus displacement (inches) for CuAS glass sample 26. Sample 26 was oxidized in air at 500°C for 30 minutes, and then reduced with 97% N_2 3% H_2 gas mixture at 500°C for 15 minutes. Tested surface of sample was polished, and then roughened with 600 grit SiC paper before treatment.
Sample Number: 26 Sample Area: 0.859 cm^2
Maximum pull stress: 171 kN/m^2

Displacement (inches)	0.000	0.002	0.004	0.006	0.008
0.00	0	40	80	130	190
0.01	260	340	420	520	620
0.02	720	810	900	960	1040
0.03	1100	1160	1200	1240	1280
0.04	1320	1350	1380	1400	1430
0.05	1450	1480	1500	1500	1320
0.06	570	470	460	460	460
0.07	460	450	240		

Table 5.31 Tape pull test force (grams) versus displacement (inches) for CuAS glass sample 27. Sample 27 was oxidized in air at 500°C for 30 minutes, and then reduced with 97% N_2 3% H_2 gas mixture at 500°C for 15 minutes. Tested surface of sample was polished, and then roughened with 600 grit SiC paper before treatment.
Sample Number: 27 Sample Area: 1.07 cm^2
Maximum pull stress: 65 kN/m^2

Displacement (inches)	0.000	0.002	0.004	0.006	0.008
0.00	0	40	80	140	190
0.01	150	300	360	420	480
0.02	540	600	660	710	340
0.03	290	280	280	280	280

Table 5.32 Tape pull test force (grams) versus displacement (inches) for CuAS glass sample 28. Sample 28 was oxidized in air at 500°C for 30 minutes, and then reduced with 97% N_2 3% H_2 gas mixture at 500°C for 15 minutes. Tested surface of sample was polished, and then roughened with 400 grit SiC paper before treatment.
Sample Number: 28 Sample Area: 1.03 cm^2
Maximum pull stress: 190 kN/m^2

Displacement (inches)	0.000	0.002	0.004	0.006	0.008
0.00	0	40	100	150	205
0.01	260	320	415	480	580
0.02	680	770	860	950	1040
0.03	1100	1170	1240	1290	1340
0.04	1390	1420	1480	1520	1560
0.05	1590	1620	1650	1680	1710
0.06	1740	1780	1805	1840	1870
0.07	1900	1930	1950	1975	1990
0.08	2000	2000	1980	1940	1905

Table 5.33 Tape pull test force (grams) versus displacement (inches) for CuAS glass sample 29. Sample 29 was oxidized in air at 500°C for 30 minutes, and then reduced with 97% N_2 3% H_2 gas mixture at 500°C for 15 minutes. Tested surface of sample was polished, and then roughened with 400 grit SiC paper before treatment.
Sample Number: 29 Sample Area: 0.99 cm^2
Maximum pull stress: 127 kN/m^2

Displacement (inches)	0.000	0.002	0.004	0.006	0.008
0.00	0	30	65	120	150
0.01	200	250	300	350	420
0.02	480	540	610	670	725
0.03	770	830	880	920	960
0.04	1000	1020	1040	1050	1060
0.05	1070	1100	1130	1150	1180
0.06	1210	1230	1260	1280	270
0.07	180				

Table 5.34 Tape pull test force (grams) versus displacement (inches) for CuAS glass sample 30. Sample 30 was oxidized in air at 500°C for 30 minutes, and then reduced with 97% N_2 3% H_2 gas mixture at 500°C for 15 minutes. Tested surface of sample was polished, and then roughened with 400 grit SiC paper before treatment.
Sample Number: 30 Sample Area: 0.99 cm^2
Maximum pull stress: 94 kN/m^2

Displacement (inches)	0.000	0.002	0.004	0.006	0.008
0.00	0	20	60	100	150
0.01	190	240	290	350	410
0.02	480	550	620	680	750
0.03	800	860	900	920	940
0.04	950	950	950	520	490

Table 5.35 Tape pull test force (grams) versus displacement (inches) for CuAS glass sample 31. Sample 31 was oxidized in air at 500°C for 30 minutes, and then reduced with 97% N_2 3% H_2 gas mixture at 500°C for 15 minutes. Tested surface of sample was polished, and then roughened with 240 grit SiC paper before treatment.
Sample Number: 31 Sample Area: 0.897 cm^2
Maximum pull stress: 151 kN/m^2

Displacement (inches)	0.000	0.002	0.004	0.006	0.008
0.00	0	70	130	200	280
0.01	370	460	560	640	730
0.02	800	880	920	990	1040
0.03	1080	1100	1130	1140	1180
0.04	1200	1220	1230	1250	1255
0.05	1240	1240	1250	1265	1280
0.06	1295	1310	1330	1350	1360
0.07	1370	1375	1380	1340	1200
0.08	1200				

Table 5.36 Tape pull test force (grams) versus displacement (inches) for CuAS glass sample 32. Sample 32 was oxidized in air at 500°C for 30 minutes, and then reduced with 97% N_2 3% H_2 gas mixture at 500°C for 15 minutes. Tested surface of sample was polished, and then roughened with 240 grit SiC paper before treatment.
Sample Number: 32 Sample Area: 0.99 cm^2
Maximum pull stress: 86 kN/m^2

Displacement (inches)	0.000	0.002	0.004	0.006	0.008
0.00	0	20	60	110	160
0.01	210	260	310	370	420
0.02	480	540	600	640	680
0.03	730	770	810	840	870
0.04	870	860	850	850	840
0.05	820	800	800	800	780
0.06	600	560			

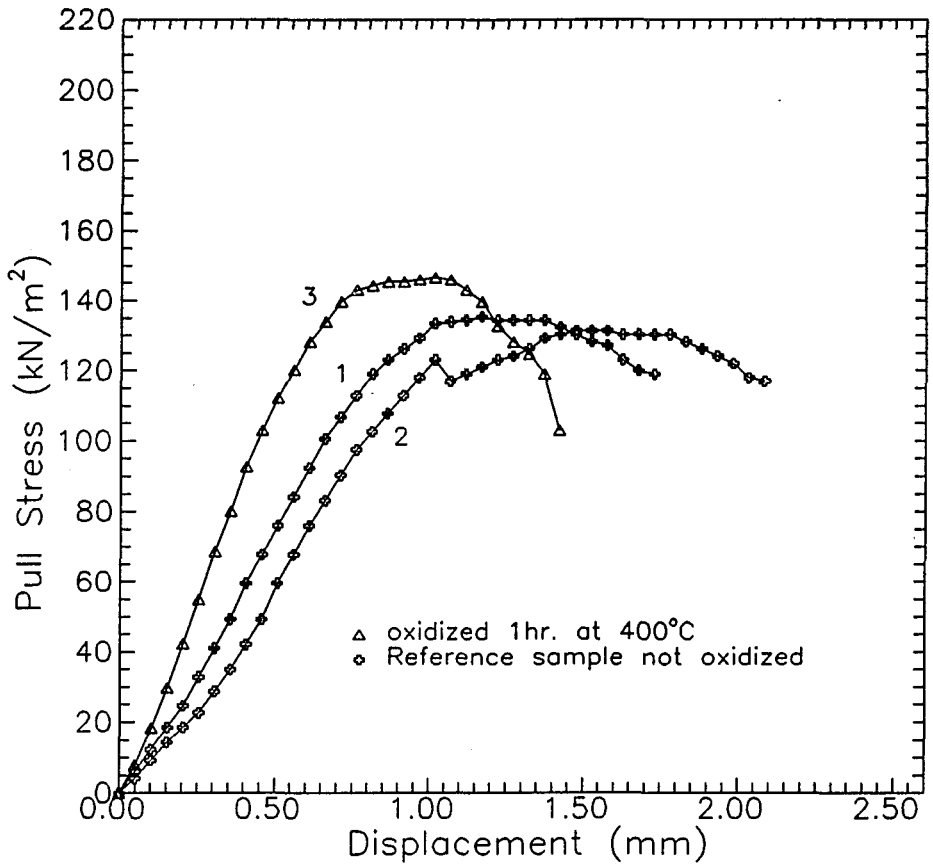

Figure 5.5 Pull test data for tape removal from polished CuAS glass (samples 1 and 2 - not thermally processed) and from CuAS glass/copper structure (sample 3). Sample 3 was processed at 400°C (oxidation time of 60 minutes).

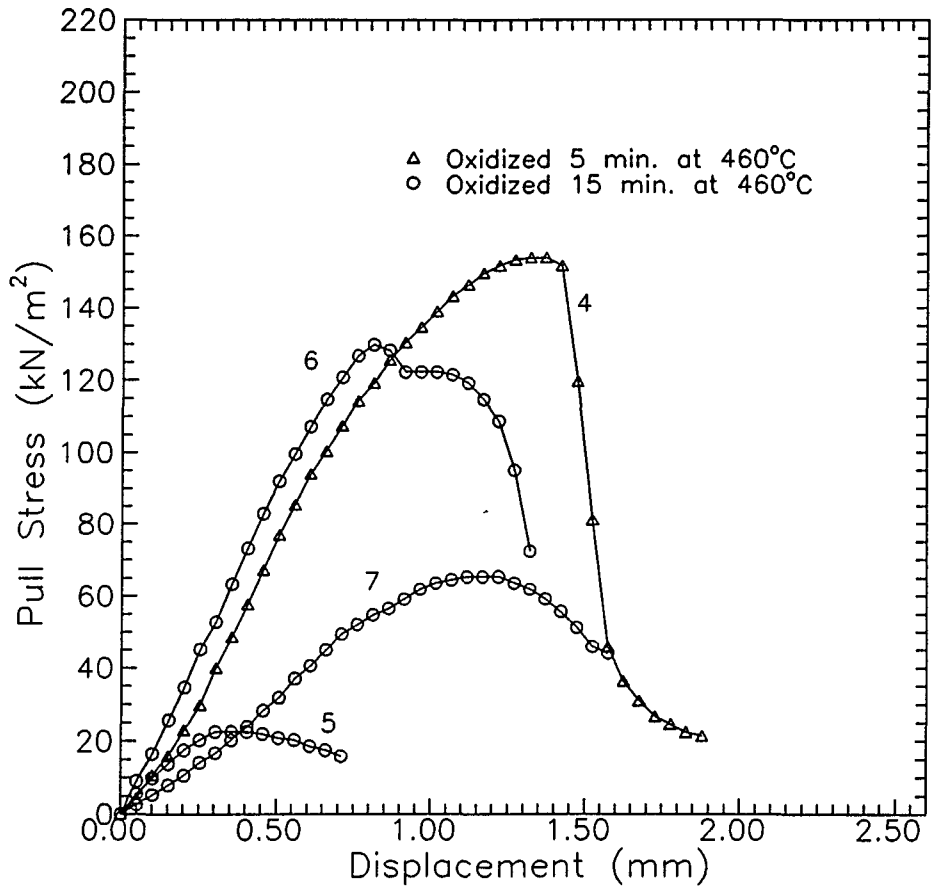

Figure 5.6 Pull test data for CuAS glass/copper structures. Data for samples 4-7 which were polished and then processed at 460°C.

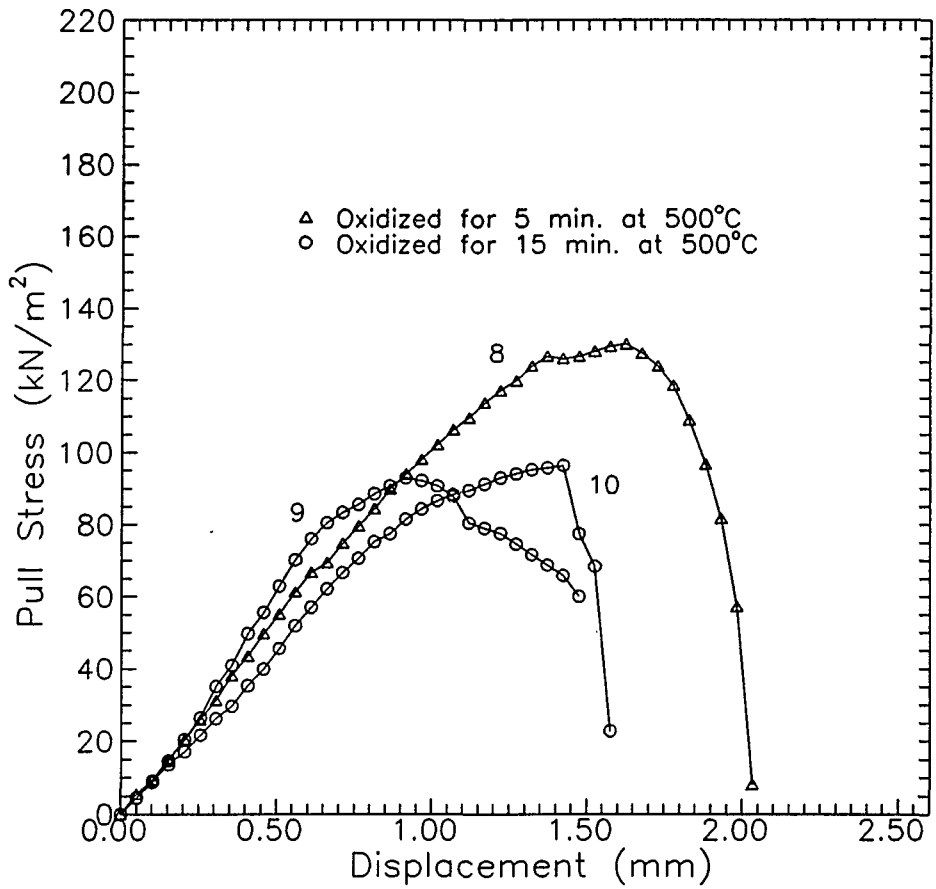

Figure 5.7 Pull test data for CuAS glass/copper structures. Data for samples 8-10 which were polished and then processed at 500°C.

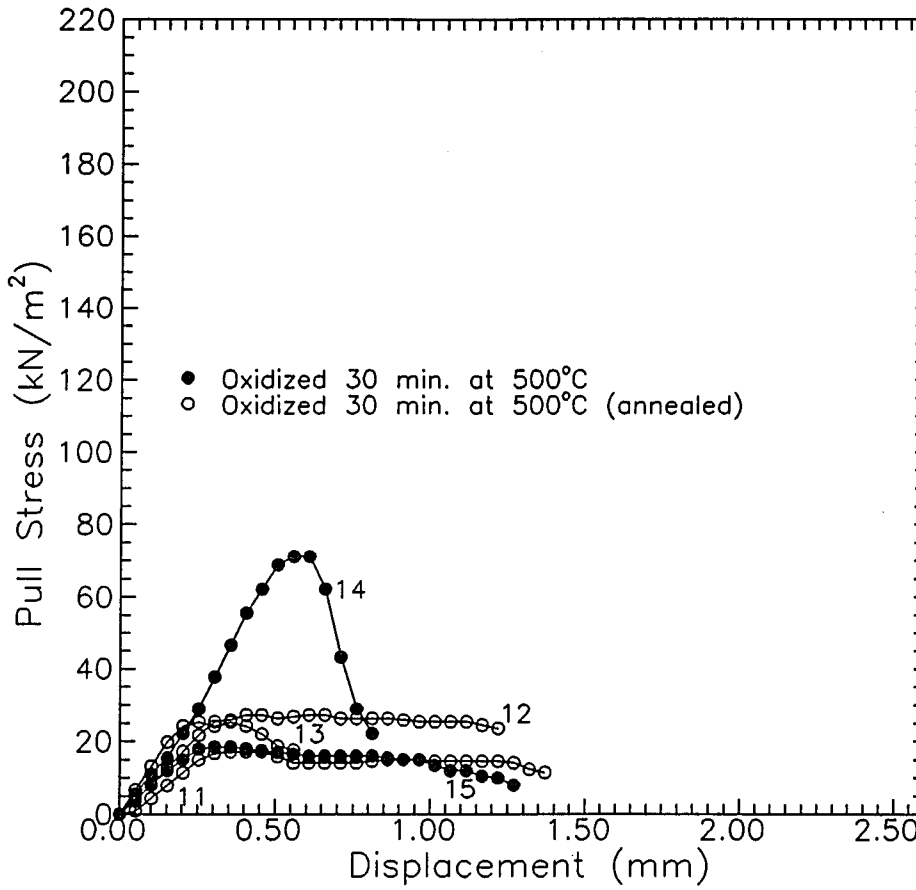

Figure 5.8 Pull test data for CuAS/copper structures. Data for samples 11-15 which were polished samples processed at 500°C (oxidation step 30 minutes).

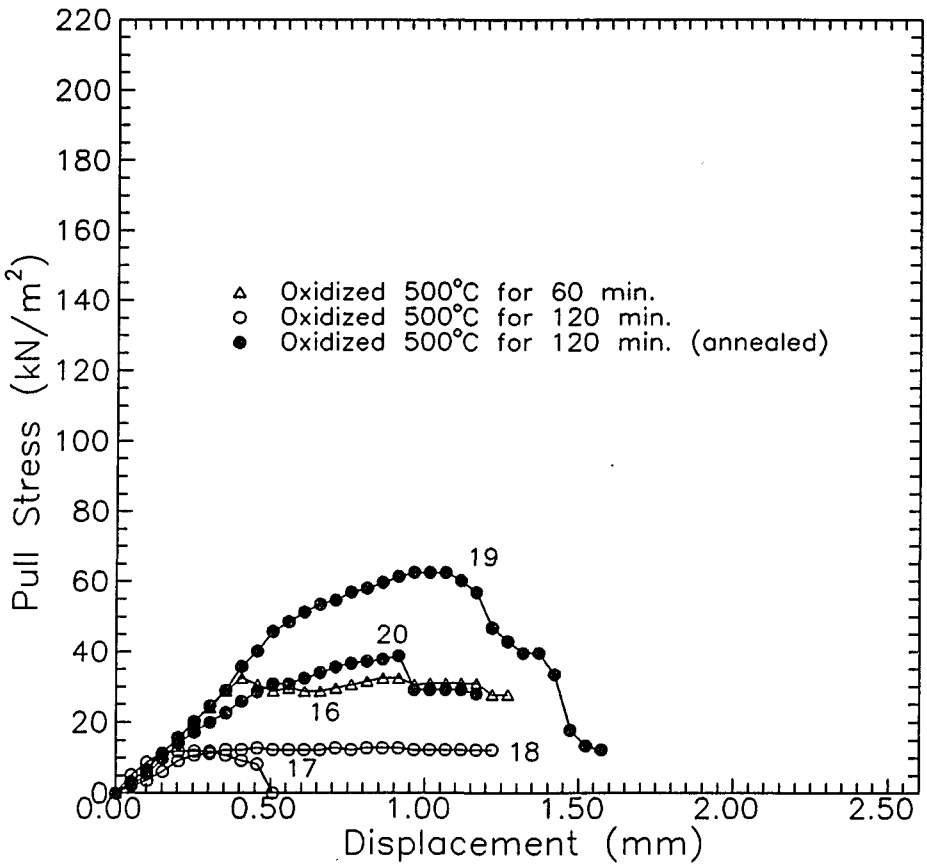

Figure 5.9 Pull test data for CuAS glass/copper structures. Data for samples 16-20 which were polished and then processed at 500°C (oxidation step 60 minutes for sample 16 and 120 minutes for all others).

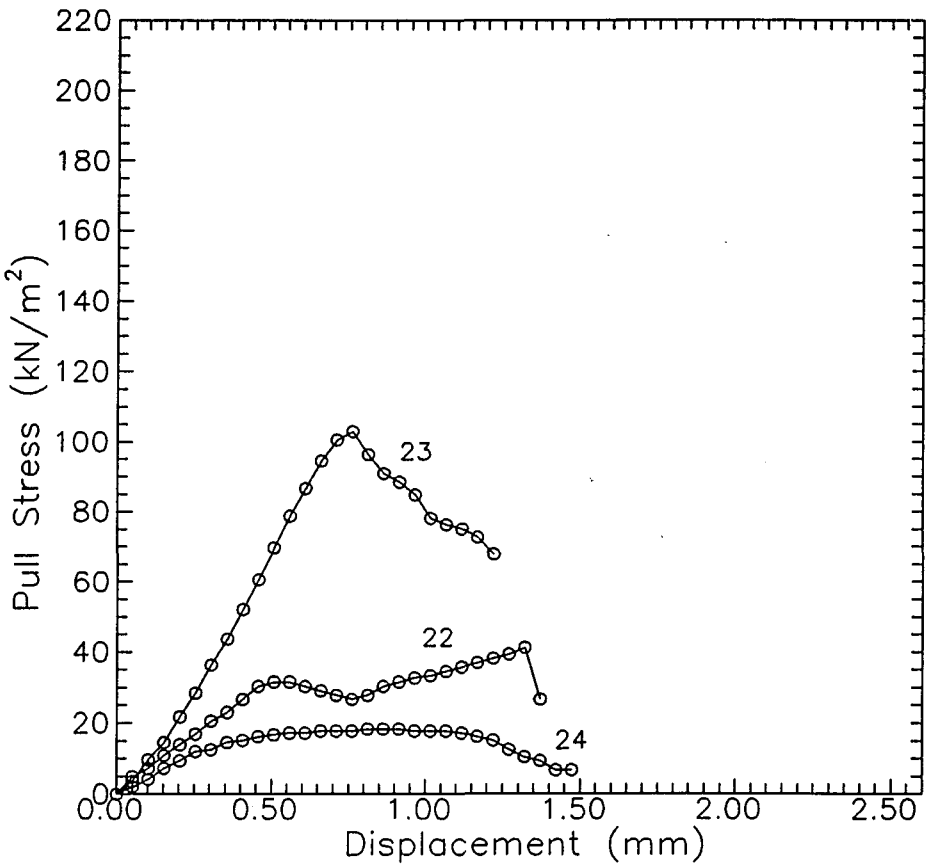

Figure 5.10 Pull test data for CuAS glass/copper structures. Data for samples 22-24 which were roughened with 1200 grit SiC paper and processed at 500°C (oxidation step was for 30 minutes).

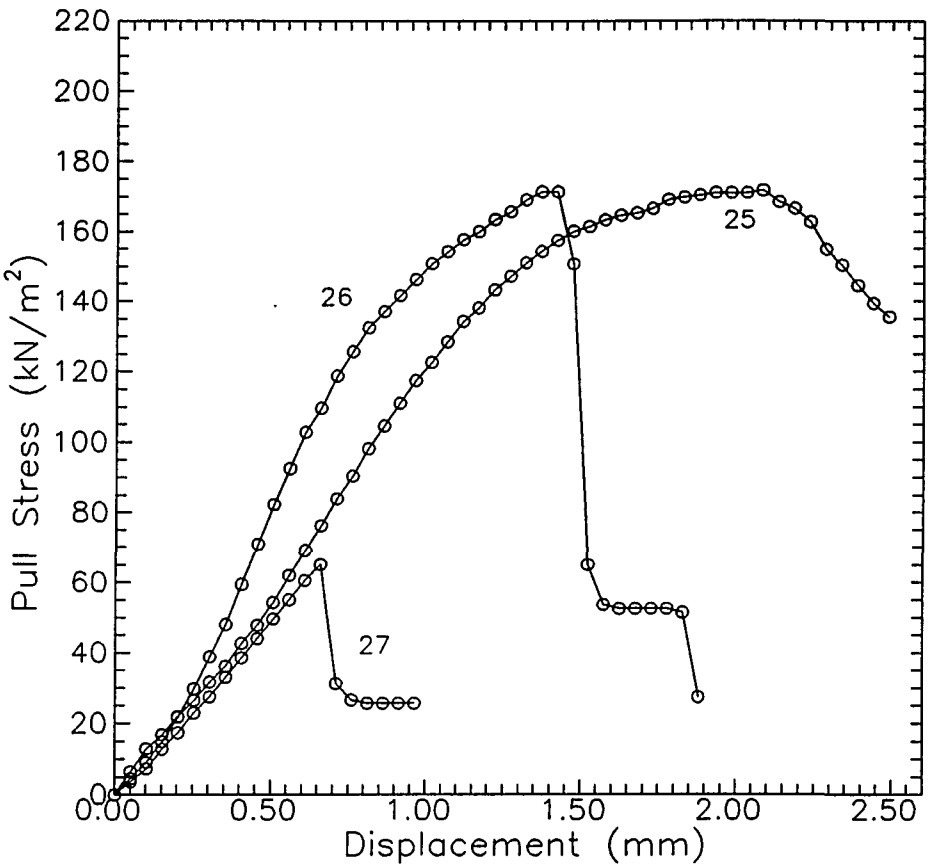

Figure 5.11 Pull test data for CuAS glass/copper structures. Data for samples 25-27 which were roughened with 600 grit SiC and processed at 500°C (oxidation step was for 30 minutes).

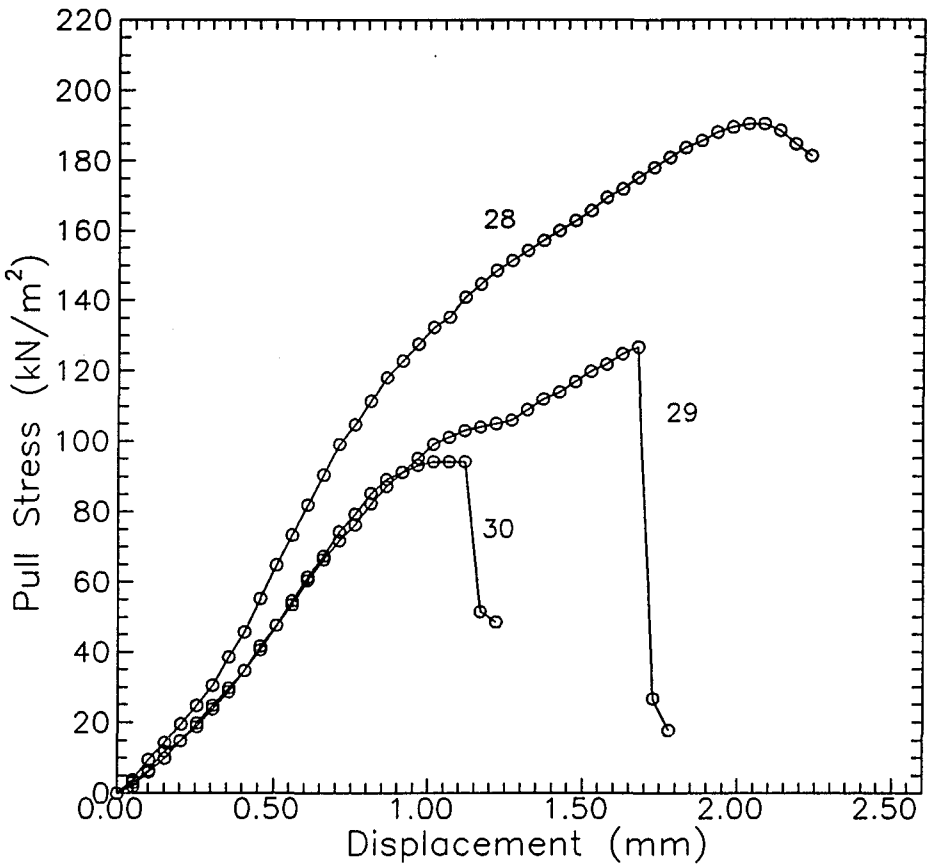

Figure 5.12 Pull test data for CuAS glass/copper structures. Data for samples 28-30 which were roughened with 400 grit SiC paper and processed at 500°C (oxidation step was for 30 minutes).

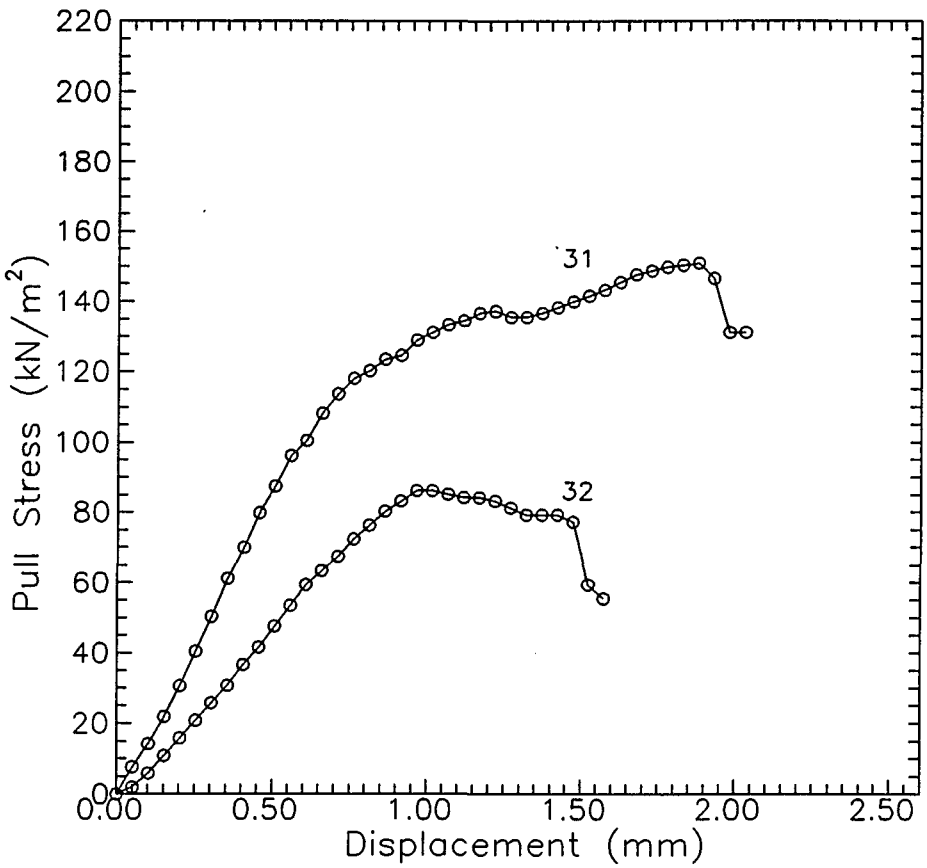

Figure 5.13 Pull test data for CuAS glass/copper structures. Data for samples 31 and 32 which were roughened with 240 grit SiC paper and then processed at 500°C (oxidation step was for 30 minutes).

CHAPTER 6

DISCUSSION

In this thesis the production of a copper aluminosilicate glass structure coated with copper film through thermal processing is studied. In this chapter the experimental results of the study are compared with relevant literature, especially the background material of this thesis, in order to characterize the processes involved. The discussion is divided into sections on the production of glass with copper in the cuprous state, the oxidation and reduction of the glass, and studies of the adhesion of the copper to the glass substrate.

6.1 Melting and Characterization of CuAS Glass

In this section, the effect of the use of alumina crucibles on the composition of CuAS glass and experiments that aided in the characterization of the CuAS glass are discussed.

Studies were completed to determine the effect of the use of alumina crucibles on the composition of CuAS glass. Figure 6.1 shows the interface between an alumina crucible and the melt. The dissolution of the silicon and copper into the intergranular regions degrades the crucible, enabling grains of the crucible to be dislodged. Small grains of alumina are found in the melt as evidenced in the micrograph. It is suggested that the intergranular regions dissolved at a faster rate than the alumina grains due to the higher silica content. Wetting of the crucible by the melt is to be expected from their similar compositions. This explains the ability

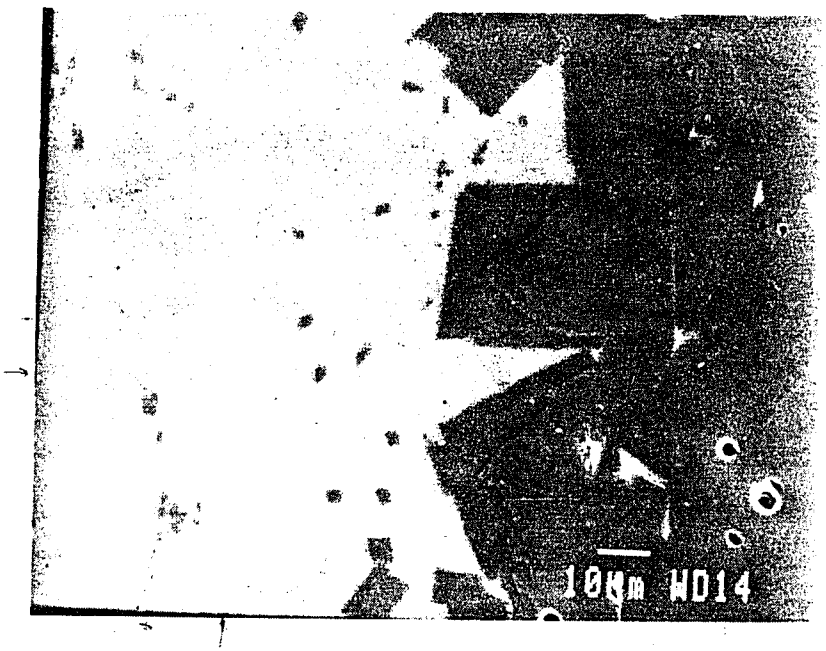

Figure 6.1 Dissolution of alumina crucible into melt. Note grains in alumina crucible are readily apparent.

of the glass to move into the crucible and fill the pores. Figure 6.2 shows an EDAX linescan for the composition of copper, alumina, and silicon across a glass/crucible interface. The scan is along the line marked in Figure 6.1, the distance being measured from the rightmost point. The large grains of alumina were found to contain nearly pure alumina. The smaller grains were found to have a greater concentration of silica. The glass which penetrated into the crucible showed elevated levels of copper. At the endpoint on the left end of the line, the glass is already approaching the batch composition for $Cu_2O{\cdot}Al_2O_3{\cdot}6SiO_2$ glass. Note that in this composition, the ratio of the metal ions copper, aluminum and silicon, is 2:2:6. Figure 6.3 shows another scan across a glass/crucible interface, measured at a magnified scale. The composition at distances greater than one half millimeter from the glass-crucible interface is close to the bulk composition. The alumina crucibles do not significantly affect the composition of CuAS glass at a sufficient distance from the glass crucible interface.

Figure 5.2 shows a DTA scan for the 1-1-6 copper aluminosilicate glass. The results were very similar to those reported by Matusita *et al.*[34] They suggested the exothermic peak corresponds to the crystallization of beta-spodumene-type crystals, and the endothermic peak to their decomposition. The peaks in this study were shifted to a higher temperature relative to their observations. This corresponds with the fact that this study used a heating rate of 10°C per minute while their study used a heating rate of 5°C per minute. In Figure 5.2, small exothermic peaks are also noticeable near 800°C. It is possible one of these corresponds to an annealing

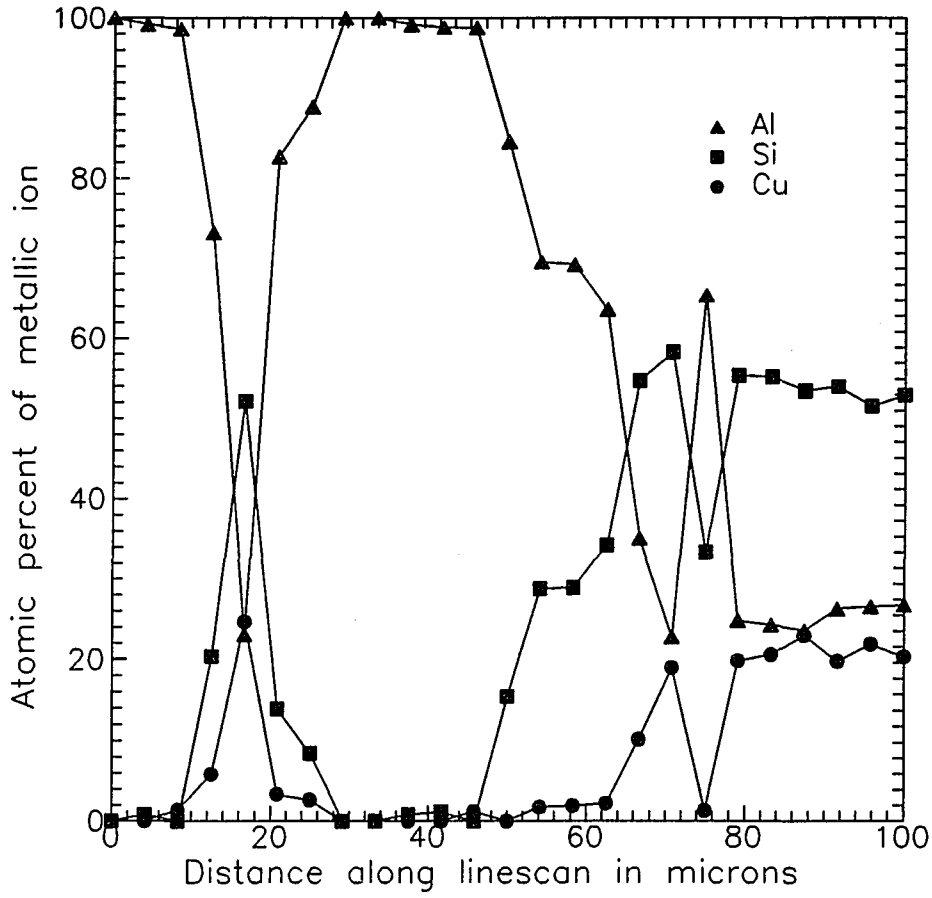

Figure 6.2 Linescan across crucible glass interface. Triangles, squares, and circles correspond to aluminum, silicon and copper respectively.

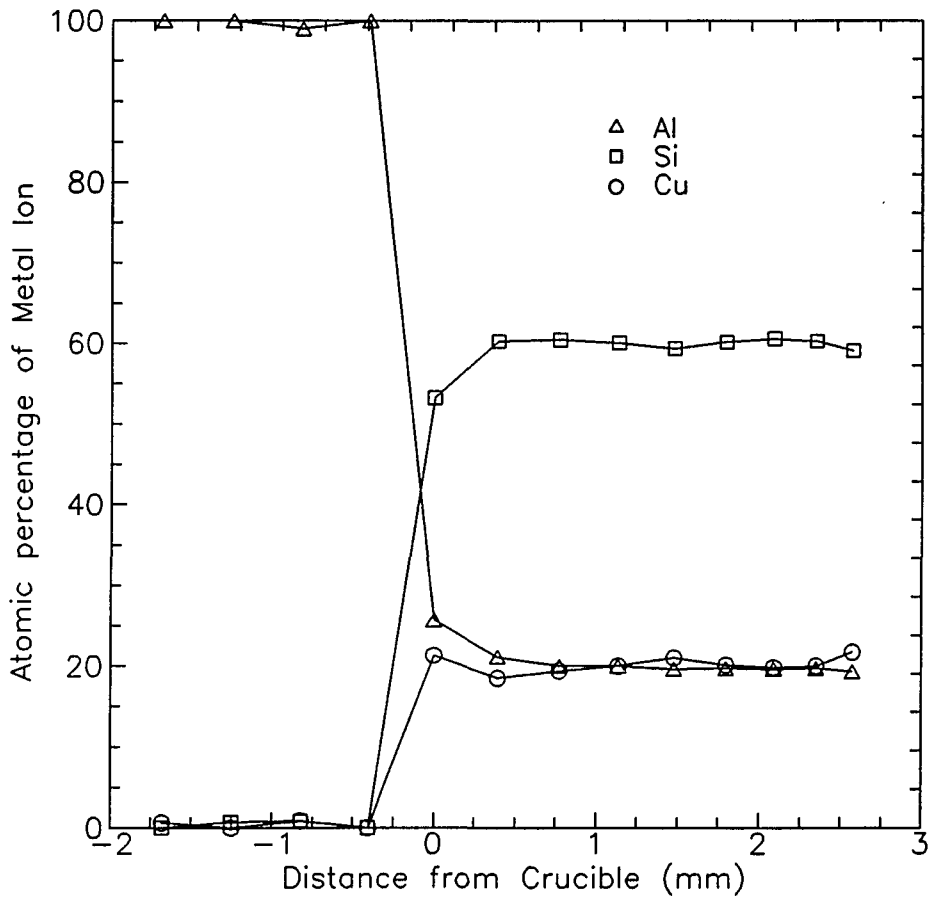

Figure 6.3 Concentration of copper, alumina and silicon in glass as a function of distance from glass/crucible interface.

relaxation. The DTA data suggest that 800°C is a suitable temperature at which to anneal 1-1-6 copper aluminosilicate glass.

The results also included qualitative features of other glass compositions produced. The ability of some of the glasses containing significant amounts of network modifiers to be poured at lower temperatures than the $Cu_2O \cdot Al_2O_3 \cdot 6SiO_2$ glass is not surprising, as the additives would be expected to lower the viscosity of the glasses. Potassium and sodium would be expected to increase the activity of oxygen in the melt, favoring the higher oxidation states of the copper.[10] It is therefore expected that the color of the glass would not change as the cupric oxide is largely responsible for the color. Tin, however, would tend to create reducing conditions in the glass. The result was a glass which had a straw color. This observation is in agreement with colors found during the production of different "ruby" glasses.[10] The effect of nickel on the melting point of the glass may be expected to be similar to the affect of copper. It was found the addition of NiO made it possible to pour the glass at 1500°C, while pouring was not successful with the 1-1-6 copper aluminosilicate glass at 1600°C. This indicates the addition of NiO lowered the melting point of the glass by over 100°C, as is the case with the addition of CuO to 1-1-6 copper aluminosilicate glass.[5]

The emission spectrum for the 1-1-6 glass (Figure 2.1) indicates most of the copper was in the Cu^{++} state as found by previous researchers. The calculations in Table 5.3 suggest that if the oxygen in the glass is in equilibrium with air, and if the cupric oxide and cuprous oxide have activities given by their molar concentration, the

amount of copper in the cuprous should increase with temperature. The value of 121 kJ per mole oxygen appears to be a reasonable value for the transformation of cuprous to cupric oxide at 1500°C.

6.2 Formation of Oxidation Layer on Glass

In this section the thermodynamic, kinetic, and structural results for the oxidation of CuAs glass are covered. A discussion of thermodynamic issues related to the formation of oxide layers on the alternate glass compositions is deferred to the next section on reduction of the oxide layer, since interpretation of oxidation relies on results found during reduction.

A cupric oxide layer was found to form on CuAS glass on heating in dry air at all temperatures from 400°C to 500°C. In Figure 6.4, the average cupric oxide layer thickness is plotted as a function of the square root of time. In order to determine an average thickness for the samples measured by the surface profile technique, a least squares fit was performed on the SEM data to find a relationship between the average height and peak height. The linear relationship determined using a least squares fit was:

$$w_{avg}=(.00359w_{max}+0.854)w_{max} \qquad (5.2)$$

where w_{avg} was the average width of the oxide layers in microns and w_{max} was the maximum width of the oxide layer in microns. The sample oxidized at 460°C for 4 hours was calculated to have an average width of 1.25 μm from a peak width of 1.46

μm. The sample oxidized at 480°C for 4 hours was calculated to have an average width of 1.7 μm from a peak width of 2.0 μm. The sample oxidized at 500°C for 1 hour was calculated to have an average width of 1.15 μm from a peak width of 1.34 μm.

The average oxide layer width plotted against the square root of time exhibits nearly linear behavior for each temperature studied, suggesting that the growth rate of the oxide layer is parabolic. The data was least squares fitted to equation (2.32) assuming that the diffusion coefficient assumed the Arrhenius form (equation (2.33)). The activation energy for diffusion was assumed to be unknown. A least-squares fit was performed using procedures outlined in section 3.3, and programs from the book *Numerical Recipes in C.*[21] The equation obtained was:

$$w = 36200 \cdot \sqrt{\exp\left(\frac{-32.2Kcal}{RT}\right) t} \qquad (5.3)$$

where w is the width of the cupric oxide layer in μm, t is the time in hours, and T is the temperature at which the sample was oxidized in Kelvin. The activation energy was calculated to be 32.2 ± 2.9 Kcal/mole (one standard deviation). The same calculation was performed excluding the surface profile data resulted in and activation energy of 32.6 ± 3.0 Kcal/mole.

From the model, the activation energy should correspond to the activation energy of the diffusing species through cupric oxide. Given that the diffusion coefficient of copper through copper oxide is an order of magnitude higher than that

for oxygen,[35] the relevant diffusing species is expected to be copper. Therefore, the activation energy determined from experiment should correspond to the activation energy of copper through cupric oxide. The activation energy of copper diffusion through cupric oxide is known to be approximately 35 kcal/mole in the temperature range 760-1125°C.[35] The predictions of the model are therefore in good agreement with experiment. Note, however, that it is not clear which type of copper vacancy is responsible for the migration of the copper. Peterson and Wiley[36] found in the case of cuprous oxide that both neutral and singly charged copper species are responsible for the diffusion of the copper. Their conclusion was based on extensive thermogravimetric, radioactive-tracer diffusion, and conductivity data.[36] Similarly it is possible that more than one type of point defect is responsible for the diffusion of copper through cupric oxide.

In the use of the above model it was assumed that depletion of copper from the glass did not affect the oxidation rate. Work done by Kamiya *et al.* showed that repeated oxidation and removal of the copper oxide layer from $Cu_2O{\cdot}Al_2O_3{\cdot}4SiO_2$ glass did not change the rate of oxidation.[7] It is expected their conclusions should hold for the oxidation of the glass composition used in this study ($Cu_2O{\cdot}Al_2O_3{\cdot}6SiO_2$). The work of Yoko *et al.*,[6] suggests that the diffusion coefficient of copper ions in CuAS glass is quite large. They used ion exchange at 550°C to alter the copper concentration in glasses. Within one hour the copper diffused a distance of the order of hundreds of μm. It is therefore reasonable to

expect the diffusion coefficient of copper ions through the CuAS glass is appreciably faster than through CuO, and will not be a rate limiting step.

Taken together, these results suggest that Kamiya's[7] model is valid: the rate of the reaction is controlled by the diffusion of copper through the oxide layer. The glass used in this study was 1-1-6 as opposed to the use by Kamiya of 1-1-4. Since the copper concentration of the glass used by Kamiya was higher, it is expected the concentration of vacancies in the oxide at the glass/oxide interface should be lower (see equation (2.14)). A lower concentration of vacancies at the glass oxide interface, $[V_m]_i$, would lead to a greater flux of copper ions (equation (2.20)) and therefore a greater growth rate (equation (2.27)). An investigation of the data of Kamiya show a layer of approximately 7.5 mg/cm^2 when a sample of glass was oxidized in air for 10 hours at 500°C.[7] Taking a density of 6.2 g/cm^3 for the cupric oxide[37], this converts to an oxide thickness of only 1.2 μm. The present study indicates that for 1-1-6 CuAS glass it would take only 1.4 hours to a reach a cupric oxide layer thickness of 1.2 μm at 500°C. There are several possible reasons for the discrepancy. Certainly it is possible that the density of the cupric oxide formed on the glass is significantly below the value of 6.2 g/cm^3, or that increasing the concentration of copper in the glass does decrease the oxidation rate. However, it is more likely the result of differences in experimental technique. In Kamiya's published work, neither the method of temperature control nor the water content of the air they used is recorded. Differences in stress and density of the glass used for their process could also cause differing oxidation rates. However, in this study

the thickness of an oxide layer grown on a sample annealed at 800°C and an unannealed glass sample were compared and found to be within 20% using DEKTAK surface profile measurements. This the stress states normally found in the CuAS glass do not have a significant effect on the oxidation rate.

Cracks formed in the cupric oxide layers during their growth and became prevalent when the thickness exceeded approximately 0.25 μm. It is suggested that the cracking was due to stresses induced in the oxide layer during growth. Cracks were sometimes found in the glass instead of the oxide layer, indicating that there was good chemical adhesion between the copper oxide layer and the glass. The cracks which formed in the Cu_2O were sometimes apparent at the processing temperature of 500°C, suggesting that there was stress associated with the production of the oxide layer. The cracks which formed in the CuAS glass are shown in Figure 6.6. Internal stresses often arise from the formation of an oxide layer on a material. Voids were also found in samples that were several μm wide. It may be expected that the cracks affected the oxide thickness measurements. However, it was possible to find regions using the SEM that were not near cracks. When the DEKTAK was used to make thickness measurements, avoiding cracks was found to be a more difficult problem. It is interesting to note the oxide was formed across the entire surface, even when the sample was rough. This suggest diffusion that growth of the oxide layer was not impeded by transport of oxygen to the surface of the oxide. This represents an advantage over other processes, such as sputtering, where "shadows" can be found related to the topography of the substrate.

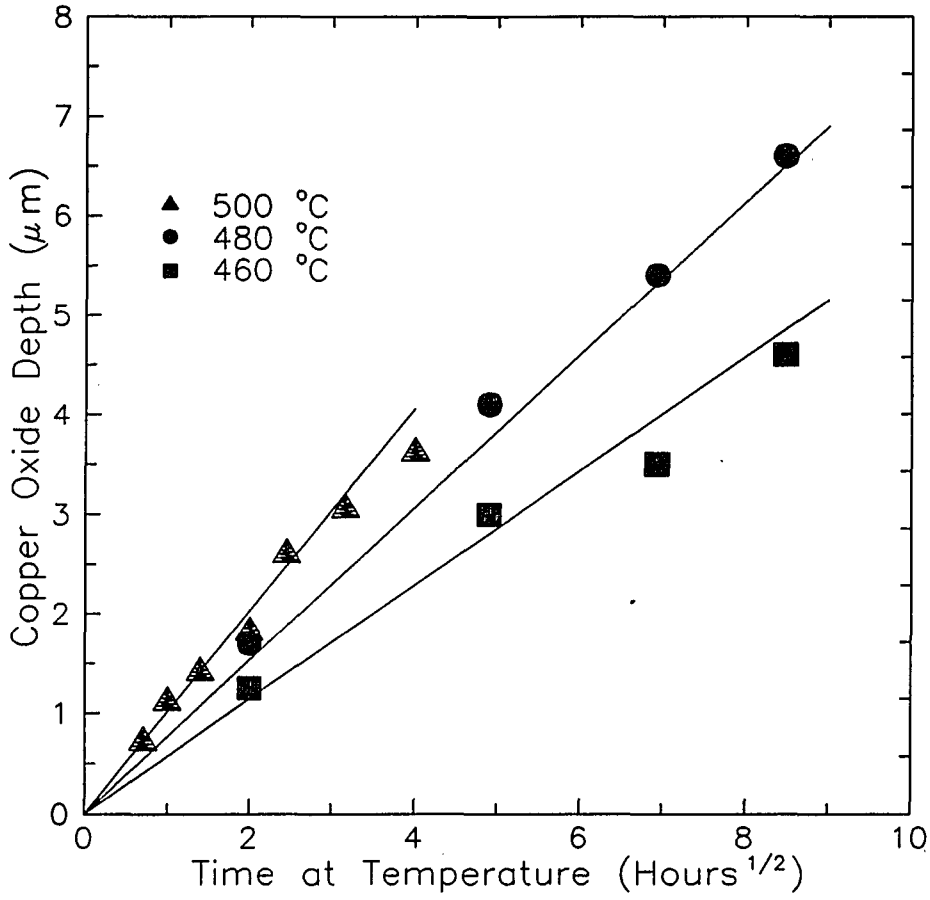

Figure 6.4 Thickness of cupric oxide layer on 1-1-6 CuAS glass function of the square root of time for oxidation at 460°C, 480°C and 500°C.

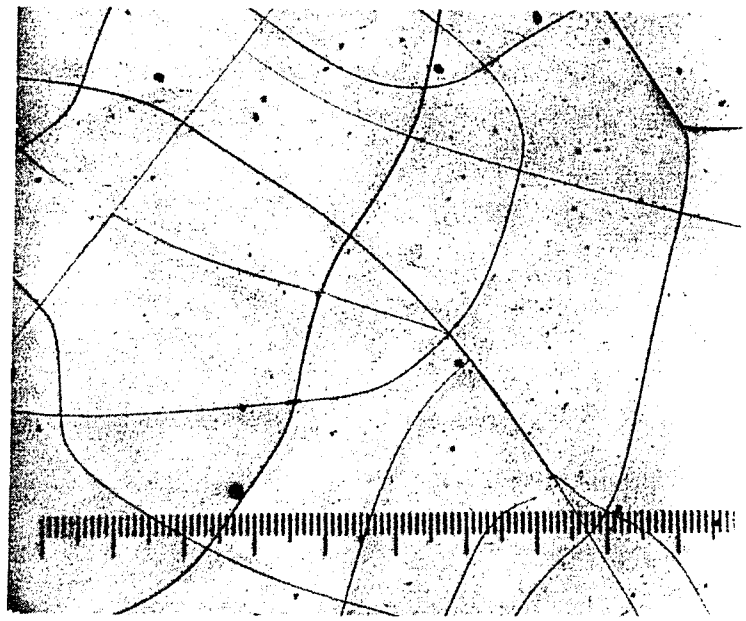

Figure 6.5 Picture of cracks formed in CuAS glass after oxidizing at 500°C for 60 minutes and reducing at 500°C for 15 minutes (copper layer was removed). Each scale division represents 20 microns.

6.3 Reduction of Oxide Layer

In this section, the energetic favorability of producing reduced copper is discussed first, followed by kinetic and structural considerations. The production of the copper layer depends on the production of the cupric oxide layer, therefore the thermodynamics of both processes will be discussed here.

All the different glasses produced an oxide film upon heating in air to 500°C. When they were reduced in air all glasses except those which contained potassium produced a highly conducting surface (resistances less than 1 ohm across a distance of approximately 0.5 cm). The production of the copper layer depended upon having glass with copper in the cuprous state and production of a cupric oxide layer with limited impurities. The rate at which copper forms the cupric oxide layer depends on the diffusion coefficient of copper, and the driving force to form a higher oxide of copper. If there are other species in the glass which are unstable relative to a higher oxidation state, and have a high diffusivity, they could be expected to be found as impurities in the oxide layer. The relative stability of oxides is given by the Ellingham diagrams in Figure 2.1 and Figure 6.6. Note, for example, the stable oxide form of nickel found at the temperature at which the glasses were melted (approximately 1500°C) is the same as that at 500°C, assuming the partial pressure of oxygen in the glass is not significantly decreased. This is also true for tin and chromium. Sodium and potassium, however, have different stable oxides over the temperature range of interest. From these thermodynamic arguments, potassium and sodium are most likely to change their oxidation state during thermal processing.

Potassium and sodium also have high diffusion coefficients in glasses[38] and therefore the reaction rates involving these species are expected to be large. The glasses produced with addition of potassium were the only glasses which lacked a conductive copper film after processing. A non-conducting layer upon reduction was not found with the sodium glass. This could, however, be due to the fact that the concentration of sodium (3 atomic percent) used was significantly lower than the concentration of potassium (20 atomic percent) used.

In order to make CuAS glass/copper structures, the CuAS glass samples were oxidized in air, and then reduced using a 97% N_2 and 3% H_2 gas mixture. The beginning of transformation of the cupric oxide to copper was on the order of the time required to replace the air in the tube with reducing gas. It was therefore not possible to separate the nucleation and growth of the copper crystals. Figure 6.7 is an SEM photograph of a copper layer formed by the reduction of a cupric oxide layer on CuAS glass. Note the high degree of porosity in the resulting layer. The porosity is expected, given that the molar volume of cupric oxide is approximately 12.4 cm^3, but the molar volume of copper is only 7.1 cm^3. Cracks were found in the copper layers corresponding to the cracks formed in the cupric oxide layers. Sometimes bridges formed across the cracks, suggesting a significant diffusion of copper. Appreciable diffusion of copper is reasonable at 500°C, the temperature at which the copper layers were formed. Another example of a copper layer formed by the reduction of a cupric oxide layer on CuAS glass is given in Figure 6.8. In this case the copper does not cover the full surface of the glass.

The process of reduction of cupric oxide to copper could occur directly in two steps: first the reduction of cupric oxide to cuprous oxide, and then the reduction of cuprous oxide to copper. The two separate steps have been previously studied. Li *et al.* studied the transition of cupric oxide films to cuprous oxide by vacuum annealing.[39] They conclude that the transformation is controlled by oxygen out-diffusion along the moving phase boundary. The transformation was found to be linear with time, but the crystalline phases were distinct, indicating that the oxygen preferred distinct valence states. They found that the grain size of the crystals increased with time. Ramanarayanan and Alonzo studied the reduction of cuprous oxide to copper in an environmental scanning electron microscope.[40] They found that copper grains nucleated within the cuprous oxide crystal after 6 minutes at 800°C. These nuclei then grew, eventually coalescing with other copper grains. The initial nucleation of the copper was postulated to depend on supersaturation of copper within the cuprous oxide crystals. The ultimate structure of the copper formed by Ramanarayanan and Alonzo is very similar to the structures found in this study. Modeling the process as occurring in two steps (which could easily overlap within the sample) is therefore quite plausible.

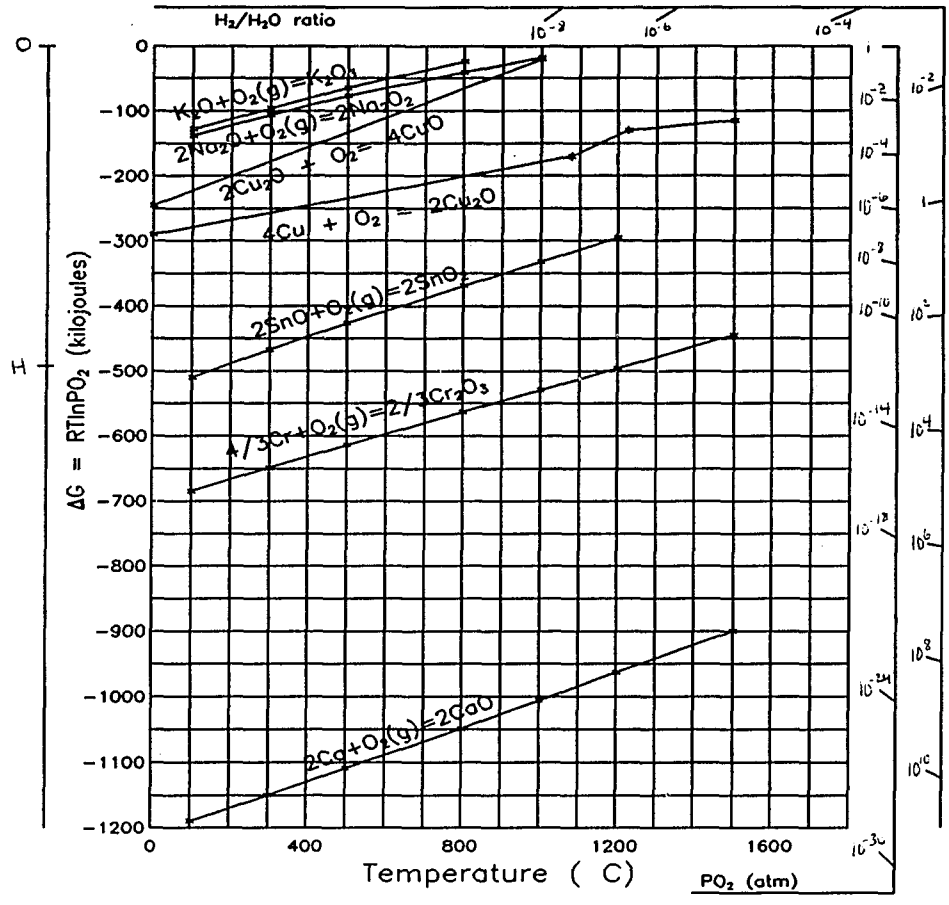

Figure 6.6 Ellingham diagram for additional oxides used in alternate glass compositions.

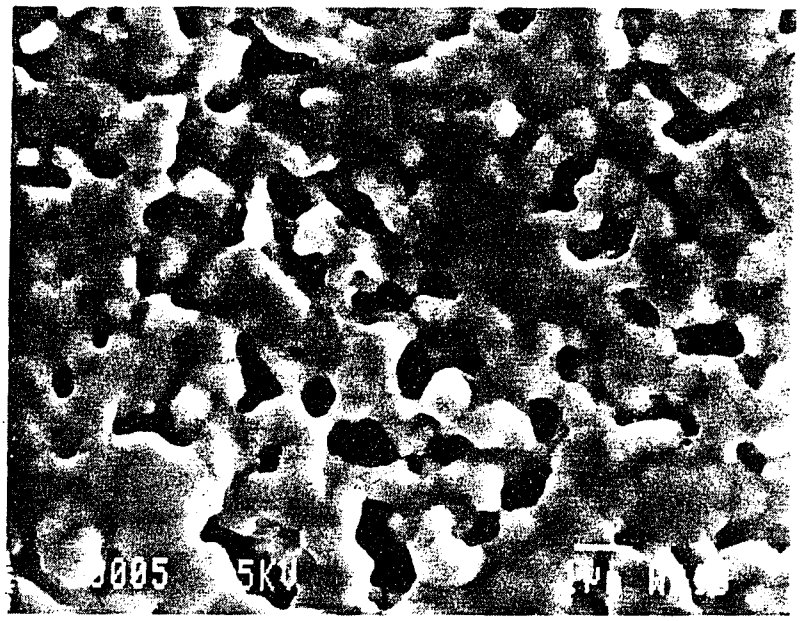

Figure 6.7 Copper formed by reduction of cupric oxide on a copper aluminosilicate substrate. Original glass sample was oxidized in air at 500°C for one hour.

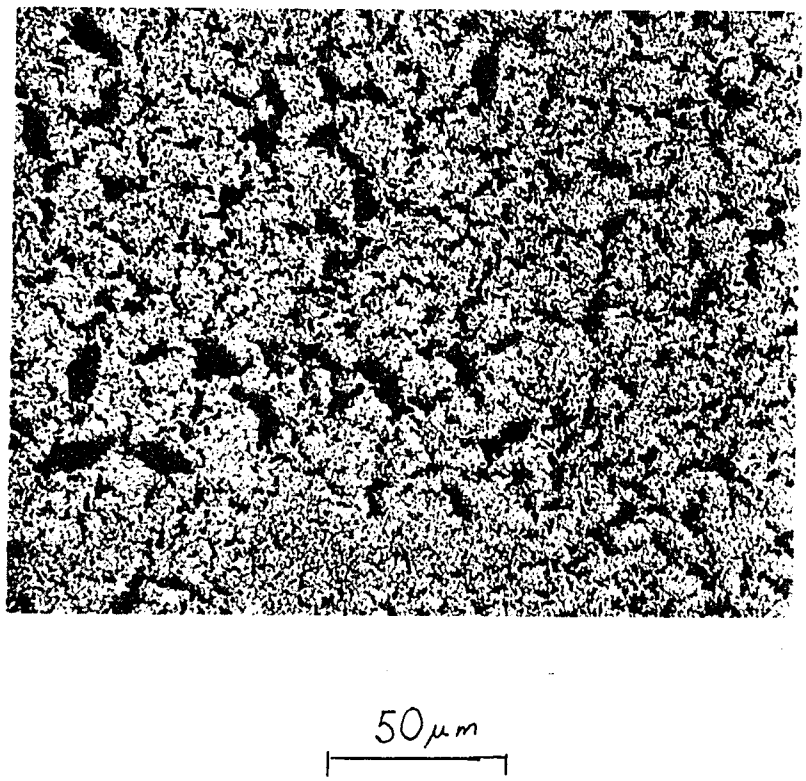

Figure 6.8 Copper film formed on CuAS glass after oxidation at 460°C for 15 minutes and subsequent reduction. Light regions are copper.

6.4 Adherence of Copper Layer to Glass Substrate

The adherence measurement technique was a combination of two techniques discussed in Chapter 3, the threshold test and the pin-pull test. Neither test is useful for calculations of the energy of adhesion between a film and a substrate, however, each has found use as a testing procedure in industry, since they provide practical information on the degree of adherence. The test used in this thesis was a pin test, with the exception that a rigid cement was not used, but a piece of tape. A rigid cement was thought undesirable because of the possibility of the cement mechanically anchoring in a roughened glass surface, irrespective of the copper film on the glass. The use of tape limited the maximum adhesive force that could be measured to the adhesive strength of the tape.

Table 6.1 is a summary of the pull test measurements for the CuAS glass/copper structures. Notice the highest pull stress were acheived by samples which were roughened before processing, such as samples 25, 26 and 28. High pull stresses were also observed with samples with a very thin or non-existant copper layer, such as samples 1, 2, 3 and 4. It therefore appears the maximum pull stress acheived is related to the roughness of the glass surface processed and also to the thickness of the copper layer produced.

Figure 6.9 shows the maximum adherence force withstood by the copper layers as a function of the thickness of the original cupric oxide layer. The graph indicates that better adhesion is achieved by a thinner copper layer. However, it is likely that the large adherence measured is due to the tape adhering directly to the glass,

because copper does not cover the entire surface when the film is sufficiently thin. This is indicated by Figure 6.8 which shows a photograph of the copper/glass structure made from the sample oxidized at 460°C for 15 minutes. Note that the glass is a large portion of the glass is not covered by the cupric oxide layer.

There is a greater strength for the annealed samples. The reason for this increased strength does not appear to be the lack of cracks, as cracks were also found in the annealed specimen. Crystallization was also not expected to be a problem as the DTA data suggest that an anneal for two hours at 800°C should not produced marked crystallization, and only a few very small crystals were observed by inspection by an optical microscope. The explanation for this phenomena is therefore not readily apparent.

Figure 6.10 gives the pull results for structures produced on glass of various roughnesses. The ultimate force endured by the samples roughened with 240 and 600 grit silicon carbide paper was approximately equal to the adherence strength of the tape to metal. The sample which was roughened with 240 grit silicon carbide paper had most of the copper remaining attached to the glass after the pulling was performed. When 600 grit paper was used, however, most of the copper was removed with the tape. The regions which were removed followed sharp lines resembling the crack lines found in the copper layer before pulling. It is concluded that roughening with 240 grit silicon-carbide paper provided the best strength, due to increased mechanical anchoring, but that cracks continued to promote failure.

Table 6.1 Summary of production parameters and pull test results for CuAS glass/copper structures.

No	Oxid-ation Temp (°C)	Oxid-ation Time (min.)	Calcu-lated thickness (μm)	Prep. Method	Max. stress (N/m^2)	Comment
1	(none)	0	0.0	polished	135	not pro-cessed
2	(none)	0	0.0	polished	131	" "
3	400	60	.21	polished	146	Copper removed
4	460	5	.14	polished	154	" "
5	460	15	.25	polished	23	" "
6	460	15	.25	polished	129	" "
7	460	15	.25	polished	65	" "
8	500	5	.30	polished	130	" "
9	500	15	.51	polished	93	" "
10	500	15	.51	polished	96	" "
11	500	30	.72	polished	17	" "
12	500	30	.72	polished	27	" "
13	500	30	.72	polished	25	" "
14	500	30	.72	annealed polished	71	" "
15	500	30	.72	annealed polished	19	" "
16	500	60	1.03	polished	32	" "
17	500	120	1.45	polished	12	" "
18	500	120	1.45	polished	13	" "

Table 6.1 - *continued*

No	Oxid-ation Temp (°C)	Oxid-ation Time (min.)	Calcu-lated thickness (μm)	Prep. Method	Max. stress (N/m^2)	Comment
19	500	120	1.45	annealed polished	62	Copper removed
20	500	120	1.45	annealed polished	39	" "
21	500	30	.72	polished etched	21	" "
22	500	30	.72	polished 1200 grit	41	" "
23	500	30	.72	" "	103	" "
24	500	30	.72	" "	18	" "
25	500	30	.72	polished 600 grit	171	mostly present
26	500	30	.72	" "	171	mostly removed
27	500	30	.72	" "	65	" "
28	500	30	.72	polished 400 grit	190	" "
29	500	30	.72	" "	127	" "
30	500	30	.72	" "	94	" "
31	500	30	.72	polished 240 grit	151	" "
32	500	30	.72	" "	86	" "

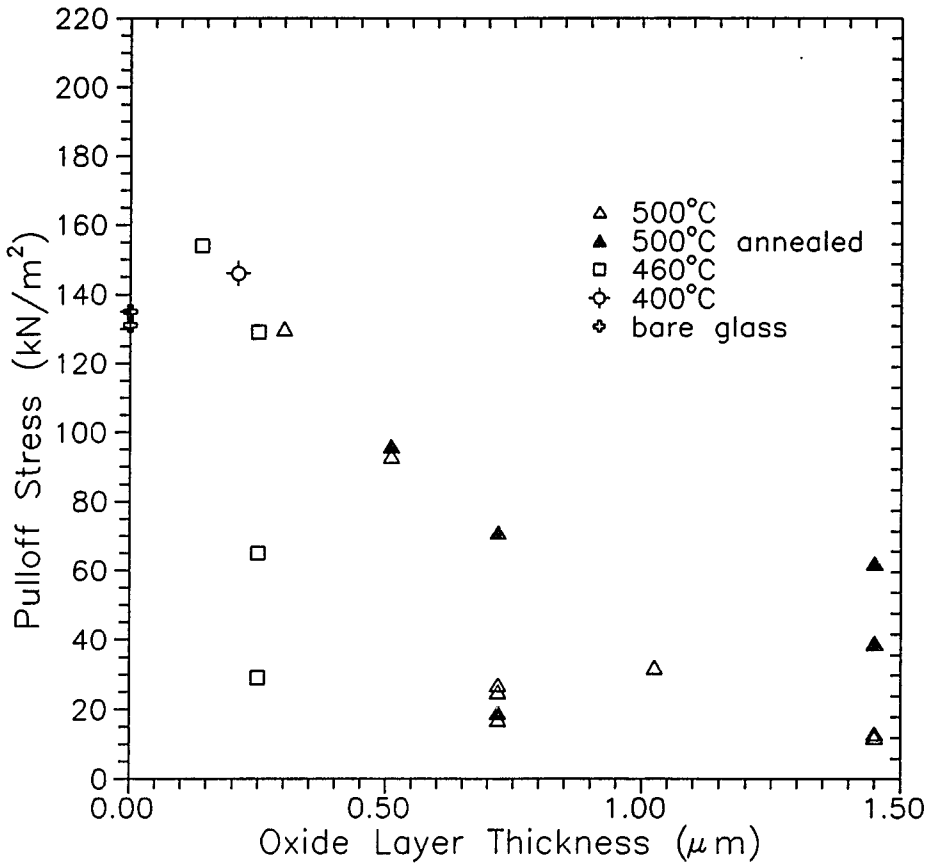

Figure 6.9 Maximum pull stress endured before rupture of copper/CuAS glass structures as a function of calculated oxide layer thickness.

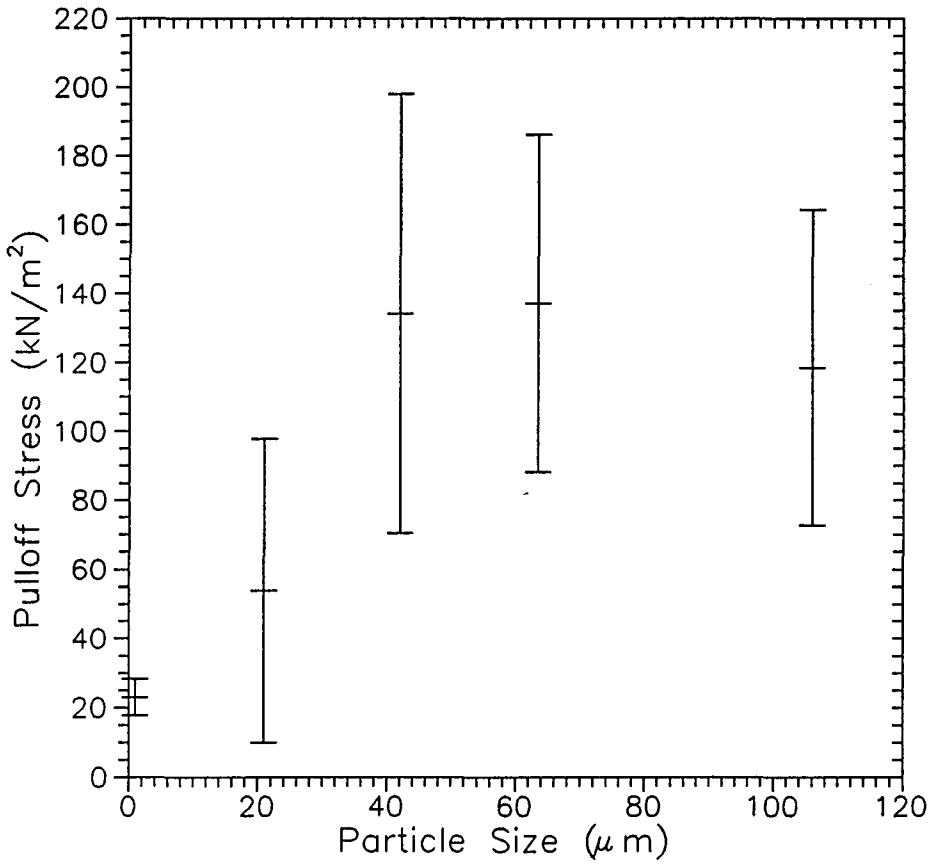

Figure 6.10 Maximum pull stress withstood by copper/CuAS glass structure versus roughness of glass substrate before processing. The polishing particles were: 1 μm diamond powder, 1200 grit, 600 grit, and 240 grit silicon carbide.

CHAPTER 7

CONCLUSION

It is possible to produce copper/CuAS glass structures by processing CuAS glass in several stages.

(1) production and processing of CuAS glass;

(2) oxidizing glass in air at temperatures near 500°C; and

(3) reducing the layer of cupric oxide on the glass.

Each of these stages of production has an important effect on the copper/copper aluminosilicate glass structures which are produced. The work of this thesis is involved with both understanding the mechanisms by which these processes operate, and practical changes that can be made in the processes in order to create improved copper/CuAS glass structures. This chapter contains conclusions concerning the mechanisms involved in each process, and practical methods by which they can be improved. The conclusions are discussed in the order of the processing stage with which they are associated.

CuAS glass can be produced by melting oxide powders in an alumina crucible up to temperatures of 1500°C. The glass dissolves away the intergranular regions of the alumina crucible at these elevated temperatures, causing grains of the crucible to be dislodged into the glass. The alumina grains also directly dissolve into the melt. For 20 ml crucibles, the compositional variations are limited to a region less than 0.5 mm from the crucible wall. Glass of composition $Cu_2O{\cdot}Al_2O_3{\cdot}6SiO_2$ produced in an alumina crucible was found to be suitable for production of

copper/CuAS glass structures. Several different oxides could be individually added to the base glass and still enable the production of copper/CuAS glass structures. These oxides included CaO, Cr_2O_3, and NiO (and also Sn metal). The addition of 10 mole percent of K_2O_3, however, did not result in a copper/CuAS glass structure using the processing steps described above.

The method by which the glass was processed had a significant impact on the integrity of the structures produced. Roughening the surface before oxidation and reduction significantly increased the adhesion of the glass to the CuAS glass substrate. There was an indication that annealing CuAS glass at 800°C before oxidation and reduction increased the adhesion of the copper layer, however, the effect was neither well established nor dramatic. Glass powders were found to be suitable for copper/CuAS glass structure production if sufficient mixing was performed in stages 2 and 3.

The oxidation of the CuAS glass followed the parabolic growth law. The activation energy of 32.5 ± 6 kcal/mole determined for the process is in good agreement with the diffusion coefficient for copper in cupric oxide. This gives additional support to Kamiya's hypothesis that the process was controlled by the diffusion of copper through the oxide layer. The oxide layer formed numerous cracks as the thickness of the oxide layer increased. These cracks remained evident in the copper/CuAS glass structures that were produced with this oxide layer.

Reduction of the cupric oxide layer on the glass substrate produced a sponge-like copper matrix, exhibiting features of the oxides (such as cracks) from which it

was formed. Copper has a molar volume that is approximately 57% that of cupric oxide, and therefore the volume shrinkage is expected. However, it was found that cupric oxide layers that were less than approximately 0.3 μm in thickness did not produce a uniform spongy copper layer; instead the copper grew in islands. This is likely to be the result of a nucleation step occurring in the transformation of cupric oxide to copper. Copper bridges were found to form over some of the cracks in the copper layer. It is reasonable to suppose that they are the result of copper diffusion, as no indications "of bridges" were found across oxide cracks.

The production of copper/CuAS glass structures is possible using three stages of processing. There are various alterations that can be made to the steps of production that have significant impact on the structures produced. The limitations of the structures produced is often related to a mechanism involved in a processing step. For example, the production of 0.1 μm layers of copper on CuAS glass substrates is limited by the nucleation of copper crystals in the reduction stage of the process. There is, however, no doubt that dramatic changes in the properties of the structures produced can be effected, given that parameters as fundamental as the composition of the glass can be changed. It is hoped that this thesis provides useful input in the pursuit of such interesting structures.

APPENDIX A

NOTATION FOR ATOMIC SITES

Kröger-Vink notation is commonly used to describe solid-state chemical reactions with information about the sites involved. There are several general descriptions of this notation scheme.[14] The purpose of this appendix is to outline the terms used in Chapter 3.

Kröger-Vink notation is a method of representing reactions relative to a standard chosen lattice, which should be is a good representation of the system at hand. If the base lattice is CuO, then the normal lattice consists of copper with a two plus (2^+) charge on a copper site, and oxygen with a two minus (2^-) charge on oxygen sites. Other arrangements are noted relative to these standard position and charges. A doubly ionized copper atom on the copper site is represented as Cu_{Cu}, since that is the standard charge and position. Primes and dots are used to describe the negative and positive charges of a site relative to the standard matrix. If a copper ion of one plus(1^+) instead of two plus (2^+) occupied a copper site it would be represented as Cu'_{Cu}, since it has a charge of negative one *relative* to the expected copper with a double plus charge. Empty sites are represented by vacancies. An empty copper site would be written as V''_{Cu}, since it is a vacancy in a copper site, with a charge negative two greater than a Cu^{++} atom. Square brackets are used to represent the concentration of different species.

In the case of glass, or an interface whose structure is unknown, the convention adopted is that the charges of species are given directly. This is more

convenient than giving the charge relative to some artificial structure. In cases where more than one structure is involved, an additional indication is needed of the type of site involved, whether it is in the glass, at the interface, or within the oxide layer.

Using these conventions it is possible to compile the following list of terms:

$O_{o\ (oxide)}$ - O^{2-} ion on oxygen site in cupric oxide.

$Cu_{Cu\ (oxide)}$ - Cu^{++} ion on copper site in cupric oxide.

$V''_{Cu\ (oxide)}$ - vacancy at copper site, with charge of 2- relative to Cu^{++} ion.

$\dot{C}u_{(glass)}$ - Cu^{+} ion residing in glass.

$\ddot{C}u_{(glass)}$ - Cu^{++} ion residing in glass.

$\dot{h}$ - an electron hole, a single positive charge.

The subscripts (glass), (oxide), and (interface) are left out when they are clear from the context. The vacancy notation is only used for the oxide phase, but the subscript (oxide) is sometimes used for clarity.

APPENDIX B

SIMILARITY SOLUTION FOR PARABOLIC GROWTH

In Chapter 3 the parabolic growth law was developed for the growth of a thin film, which assumed that the migrating species was uncharged, and that the diffusion coefficient was independent of concentration. However, there was a constant, γ, in the final expression (equation (2.27)) which was not determined. In this appendix a relation for the value of γ is derived.[20,41]

Recall the following expressions from Chapter 3:

$$\left(\frac{\partial[V_M]}{\partial x}\right)_{x=w(t)} = \gamma \frac{[V_M]_s - [V_M]_i}{w} \tag{2.23}$$

$$D_M c_M^S = D_v [V_M]_s \tag{2.25}$$

$$w = \sqrt{2D_M \gamma \frac{[V_M]_s - [V_M]_i}{[V_M]_s} t} \tag{2.27}$$

Substituting equation (2.25) into equation (2.27) gives the parabolic growth law in the form:

$$w = \sqrt{2D_V \gamma \frac{[V_M]_s - [V_M]_i}{C_M^S} t} \tag{B.1}$$

With the substitutions:

$$a = c_M^S + [V_m]_s - [V_M]_i \qquad b = c_M^S \tag{B.2}$$

equation (B.1) becomes:

$$w = \sqrt{2D_v \gamma \frac{(a-b)}{b} t} \tag{B.3}$$

In equation (2.23), γ is defined in terms of the concentration gradient of vacancies at the surface of the oxide and the vacancy concentration at the oxide interface and oxide surface. Noting that the concentration gradient of vacancies is opposite to the concentration gradient of the metal ions, and using the definitions for a and b, the following relation can be derived:

$$\left(\frac{\partial c(x,t)}{\partial x}\right)_{x=w(t)} = \left(\frac{-\partial [V_m]_s}{\partial x}\right)_{x=w(t)} = \left(\frac{-\gamma([V_M]_s - [V_M]_i)}{w(t)}\right) = -\gamma \frac{(a-b)}{w(t)} \tag{B.4}$$

from which:

$$\gamma = \left(\frac{-\partial c(x,t)}{\partial x}\right)_{x=w(t)} \frac{w(t)}{(a-b)} \tag{B.5}$$

The value of γ can be determined if one can find the solution for the concentration gradient as a function of position and time. Solving for the concentration profile involves solving the diffusion equation with a moving boundary. One method of restricting the problem is to find a solution that remains similar with

respect to time, i.e. the concentration at a position x and time t depends only on the ratio of x to the thickness of the layer at time t. This leads to the definition of a normalized variable s (this is a simpler form of a transformation used by Landau[42]), which ranges from zero at the glass/oxide interface to unity at the surface of the oxide. Since the thickness of the layer at time t is $w(t)$, s is given by:

$$s = \frac{x}{w(t)} \tag{B.6}$$

Similarity also leads to the condition:

$$c(x,t) = c(s\,w(t'),t') \tag{B.7}$$

which holds for any time t'. The width of the interface is given by equation (B.3) which can be simplified by the introduction of the variable p:

$$p = \gamma\left(\frac{a-b}{b}\right) \tag{B.8}$$

Substituting the time at which the width of the interface is one for t, leads to the equation:

$$c(x,t)=c\left(s,\frac{1}{2D_v p}\right) \tag{B.9}$$

Therefore, the concentration profile can be expressed as a function of the single variable *s*. The function *y(s)* is defined:

$$y(s) = c(x,t) \tag{B.10}$$

The function *y(s)* is assumed to be a solution of the one dimensional form of Fick's second law:

$$\frac{\partial y(s)}{\partial t} = \frac{\partial}{\partial x}\left(D_v \frac{\partial y(s)}{\partial x}\right) \tag{B.11}$$

In order to find the partial derivatives of *y(s)* with respect to *x* and *t*, the relation between *s*, *x* and *t* is needed. Using equations (B.3), (B.8) and (B.6), the following is obtained:

$$s = \frac{x}{\sqrt{2D_v tp}} \tag{B.12}$$

For the partial derivative of *y(s)* with respect to *t*:

$$\frac{\partial(y(s))}{\partial t} = \frac{\partial(y(s))}{\partial s}\frac{\partial s}{\partial t} = \frac{\partial y(s)}{\partial s}\left(\frac{-x}{2t}\frac{1}{\sqrt{2D_v tp}}\right) \tag{B.13}$$

The partial derivative with respect to position, since the diffusion coefficient is assumed not to depend on position, is given by:

$$\frac{\partial}{\partial x}\left(D_v \frac{\partial y(s)}{\partial x}\right) = D_v \frac{\partial}{\partial s}\left(\frac{\partial y(s)}{\partial s}\frac{\partial s}{\partial x}\right)\frac{\partial s}{\partial x} = D_v \frac{\partial^2 y(s)}{\partial s^2}\frac{1}{2D_v tp} \tag{B.14}$$

Substituting back into Fick's second law:

$$\frac{D_v}{2Dtp}\frac{\partial^2 y(s)}{\partial s^2} + \frac{x}{2t}\frac{1}{\sqrt{2tpD_v}}\frac{\partial y}{\partial s} = 0 \qquad \text{(B.15)}$$

The final result is the following differential equation that depends only a single variable s:

$$\frac{\partial^2 y(s)}{\partial s^2} + ps\frac{\partial y(s)}{\partial s} = 0 \qquad \text{(B.16)}$$

The solution of equation (B.16) is:

$$y(s) = \int_0^s C_1 \exp\left(\frac{-pk^2}{2}\right)dk + C_2 \qquad \text{(B.17)}$$

Making use of the boundary conditions $y(0)=a$ and $y(1)=b$, the constants for the solution are determined to be:

$$C_2 = a \; ; \quad C_1 = \frac{\sqrt{2p}}{\sqrt{\pi}}\frac{(b-a)}{erf(\sqrt{p/2})} \qquad \text{(B.18)}$$

where,

$$erf(x) = \frac{2}{\sqrt{\pi}}\int_0^x \exp(-t^2)dt \; ; \qquad \text{(B.19)}$$

Inserting the constants back into equation (B.17) and again making the substitution of $-t^2$ for $-pk^2/2$ leads to the solution:

$$y = \frac{(b-a)\,erf\left(s\sqrt{\frac{p}{2}}\right)}{erf\left(\sqrt{\frac{p}{2}}\right)} + a \qquad \text{(B.20)}$$

Using equations (B.5), (B.6), (B.8), and (B.10), the following relation between p and the function $y(s)$ is found:

$$p = \left(\frac{-\partial y(s)}{\partial x}\right)_{x=w(t)} \frac{w}{b} = -\left(\frac{\partial y(s)}{\partial s}\right)_{s=1} \frac{\partial s}{\partial x} \frac{w}{b} = -\left(\frac{\partial y(s)}{\partial s}\right)_{s=1} \frac{1}{b} \qquad \text{(B.21)}$$

It is now required to relate p to a and b. Using equations (B.20) and (B.21):

$$p = \frac{(a-b)}{b} \frac{\frac{\partial}{\partial s}\left(\frac{2}{\sqrt{\pi}} \int_0^{s\sqrt{\frac{p}{2}}} \exp\left(-t^2\right) dt\right)_{s=1}}{erf(\sqrt{p/2})} \qquad \text{(B.22)}$$

Making the substitution:

$$t = v\sqrt{\frac{p}{2}} \qquad \text{(B.23)}$$

and applying the fundamental theorem of calculus:

$$\frac{\partial}{\partial x}\left(\int_0^x f(t)dt\right) = f(x) \tag{B.24}$$

equation (B.22) becomes:

$$p = \sqrt{\frac{2p}{\pi}}\ \frac{\exp(-\frac{p}{2})}{erf(\sqrt{p/2})}\ \frac{(a-b)}{b} \tag{B.25}$$

Or,

$$\frac{(a-b)}{b} = \sqrt{\frac{\pi}{2p}}\, erf(\sqrt{p/2})\exp(\frac{p}{2}) = \sqrt{\frac{\pi p}{2}}\ erf\left(\sqrt{\frac{p}{2}}\right)\exp\frac{p}{2} \tag{B.26}$$

From equation (B.26) *(a-b)/b* can be found as a function of *p*. γ is related to p by equation (B.8) which can be rewritten as:

$$\gamma = \frac{bp}{a-b} \tag{B.27}$$

From this equation one can find γ from *a,b*, and *p*. Therefore, through the use of *p*, a relation between γ and *(a-b)/b* can be found. The results of this calculation are given in Figure 2.1. The rate of growth of the oxide layer can be determined from *a*, *b*, D_v , with the use of Figure 2.1 and equation (B.3).

Note that γ approaches its maximum value of unity as *(a-b)/b* approaches zero. In this case the concentration profile within the oxide layer approaches linearity.

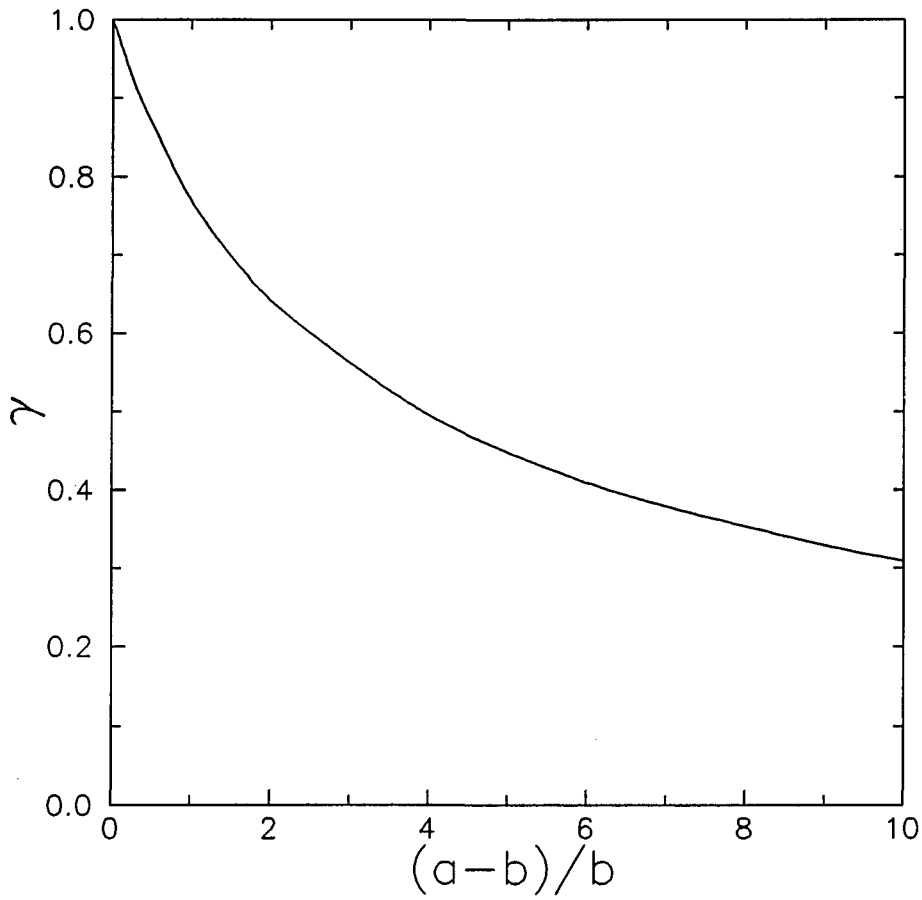

Figure 2.1 γ as a function of b/(a-b). γ is the ratio between the true slope at the surface of the oxide to the average slope through the oxide.

REFERENCES

1. N.T.E.A. Baak and C.F.Rapp, US Patent 3 498 876 (1970)

2. N.T.E.A. Baak and C.F. Rapp, US Patent 3 528 8292 (1970)

3. N.T.E.A. Baak and C.F. Rapp, US Patent 3 779 781 (1973)

4. K. Matusita and J.D. Mackenzie, J. Non-Crystalline Solids, vol. 30 (1979), pp. 285-292

5. K. Matusita, S. Sakka, and T. Shoji, J. American Ceramic Soc., vol. 66 (1983), pp. 33-35

6. T.Yoko, K. Kamiya, and S. Sakka, J. Non-Crystalline Solids, vol. 71 (1985), pp. 245-251

7. K. Kamiya, T. Yoko, and S. Sakka, J. Non-Crystalline Solids, vol. 80 (1986), pp. 405-411

8. D.C. Lynch and W.G. Davenport, *Copper Aluminosilicate Glasses and Glass-Ceramics, a Potential Market for Refined Copper*, Proposal submitted to the University of Arizona Copper Research Center, 1989, pp. 1-11

9. J. Kim, K.S. Kim, and Y.H. Kim, J. Adhesion Sci. Tech., vol. 3, no. 3 (1989), pp. 175-187 10. A. Paul, *Chemistry of Glasses*, 2nd ed., Chapman and Hall, New York, 1990, pp. 219-229

10. A. Paul, *Chemistry of Glasses*, 2nd ed., Chapman and Hall, New York, 1990, pp. 219-229

11. M.B. Volf, *Chemical Approach to Glass*, Elsevier, New York, 1984, pp. 411-415

12. D.R. Gaskill, *Introduction to Metallurgical Thermodynamics*, 2nd ed., Hemisphere Publishing Corp., New York, 1981, pp. 261-267

13. G.H. Frischat, *Ionic Diffusion in Oxide Glasses*, Trans Tech Publications, Bay Village, Ohio, 1975, pp. 1-4

14. W.D. Kingery, H.K. Bowen and D.R. Uhlmann, *Introduction to Ceramics*, John Wiley and Sons, New York, 1976, pp. 127-129

15. D.W. Bridges and W.M. Fassell, Oxidation of Metals, vol. 1, no. 2 (1969),pp. 411-415

16. E. Iguchi, K. Yajima, and Y. Saito, Trans. Japan Institute of Metals, vol. 14, no. 6 (1973), pp. 423-430

17. P. Kofstad, *High-Temperature Oxidation of Metals*, John Wiley and Sons, New York, 1966, pp. 113-123

18. F.A. Kröger, *The Chemistry of Imperfect Crystals*, vol 3., 2nd ed., American Elsevier Pub. Co., New York, 1974, pp. 72-77

19. A.T. Fromhold, Jr., J. Phys. Chem. Solids, vol. 24, (1963), pp. 1081-1092

20. J. Crank, *The Mathematics of Diffusion*, 2nd ed., Clarendon Press, Oxford, 1975, pp. 286-325

21. W.H. Press, B.T. Flannery, S.A. Teukolsky, and W.T. Vetterling, *Numerical Recipes in C the Art of Scientific Computing*, Cambridge University Press, New York, 1988, pp. 517-565

22. A.T. Fromhold Jr., "Stress and Strain in Growing Oxide Films" in *Stress Effects and the Oxidation of Metals*, J.V. Cathcart (ed.), The Metallurgical Society of AIME, New York, 1975, pp. 2-74

23. C. Roy and B. Burgess, Oxidation of Metals, vol. 2, no. 3 (1970), pp. 235-261

24. H.K. Pulker, *Coatings on Glass*, Elsevier, Amsterdam, 1984

25. D.S. Rickerby, Surface and Coatings Technology, vol. 36 (1988), pp. 541-557

26. E. Abonneau, G. Fuchs, M. Treilleux, and A. Perez, J. of Adhesion Science Tech., vol. 5, no. 12 (1991), pp. 1017-1021

27. J.C. Lambropoulos and S. Wan, "Stress in Anisotropic Thin Films Bonded to Stiff Substrates," in *Electronic Packaging Materials Science III*, R. Jaccodine, K. Jackson, and R. Sundahl (eds.), Materials Research Society, Pittsburgh, 1988, pp. 399-403

28. J.E.E. Baglin, "Interface Design for Thin Film Adhesion," in *Fundamentals of Adhesion*, L. Lee (ed.), Plenum Press, New York, 1991, pp. 363-382

29. R.J. Good, "Locus of Failure and its Implications for Adhesion Measurement," in *Adhesion Measurement of Thin Films, Thick Films, and Bulk Coatings*, K.L. Mittal (ed.), ASTM, Philadelphia, 1978, pp. 18-29

30. S. Krongelb, "Electromagnetic Tensile Adhesion Test Method," *Adhesion Measurement of Thin Films, Thick Films, and Bulk Coatings*, K.L. Mittal (ed.), ASTM, Philadelphia, 1978, pp. 107-119

31. M. Bortz and F.S. Ohuchi, "Metal-Ceramic Interfacial Reactions: The Copper-Cordierite and Titanium Cordierite Systems," in *Adhesion in Solids*, D.M. Mattox, J.E.E. Baglin, R.J. Gottshcall, and C.D. Batich (eds.), Materials Research Society, Pittsburgh, 1988, pp. 167-170

32. K.W. Paik and A.L. Ruoff, J. Adhesion Sci. Technology, vol. 4, no. 6 (1990) pp. 465-474

33. C.D. Wagner, W.M. Riggs, L.E. Davis, and J.F. Moulder, *Handbook of X-ray Photoelectron Spectroscopy (A Reference Book of Standard Data for Use in Electron Spectroscopy)* G.E. Mulenberg (ed.), Perkin-Elmers Corp. Physical Electronics Division, Eden Prairie, Minn, 1979

34. K. Matusita, J.D. Mackenzie, K. Kamiya and S. Sakka "Low Expansion Glass-Ceramics Prepared from Cu_2O-Al_2O_3-SiO_2 Glasses," *Advances in Ceramics #4*, American Ceramic Society, Westerville, Ohio, 1981, pp. 277-286

35. A.G. Revesz and F.P. Fehlner, Oxidation of Metals, vol. 15 nos. 3/4 (1981), pp. 297-320

36. N.L. Peterson and C.L. Wiley, J. Phys. Chem. Solids, vol. 45, no. 3 (1984), pp. 281-294

37. *CRC Handbook of Chemistry and Physics*, 71st ed., D.R. Lide (ed.), The Chemical Rubber Company, Boston, 1991, p. 4-62

38. G.H. Frischat, *Ionic Diffusion in Oxide Glasses*, Trans Tech Publications, Bay Village, Ohio, 1975, pp. 47-56

39. J. Li S.Q.Wang , J.W. Mayer, and K.N. Tu, Physical Review B, vol. 39, no. 16 (1989), pp. 12367-12370

40. T.A. Ramanarayanan and J. Alonzo, Oxidation of Metals, vol. 24, nos. 1/2 (1985), pp. 17-27

41. G.S.H Lock, *The Growth and Decay of Ice*, Cambridge University Press, New York, 1990, pp. 81-83

42. H.G. Landau, Q. Applied Math., vol. 8, no. 81 (1950), pp. 81-82